Hydrogeological and geochemical characterization of groundwater in the F'Kirina plain (Eastern Algeria)

Rahal Omar[a,b], Gouaidia Layachi[a], Fidelibus Maria Dolores[b*], Marchina Chiara[c] , Natali Claudio[d], Bianchini Gianluca[e],

[a]Laboratory of Sedimentary environment and mineral and water resources in eastern Algeria, Department of Earth Sciences, Larbi Tebessi University, Route de Constantine, 12002, Tébessa, Algérie, omar.rahal@univ-tebessa.dz, layachi.gouaidia@univ-tebessa.dz
[b]Dipartimento di Ingegneria Civile, Ambientale, del Territorio, Edile e di Chimica, Politecnico di Bari, Via Orabona 4, 70125, Bari, Italy, mariadolores.fidelibus@poliba.it
[c]Dipartimento Territorio e Sistemi Agro-Forestali, Università degli Studi di Padova, Viale dell'Università 16, 35020, Legnaro (Padova), Italy, chiara.marchina@unipd.it
[d]Dipartimento di Scienze della Terra, Università di Firenze, Via La Pira 4, 50121, Firenze, Italy, claudio.natali@unifi.it
[e]Dipartimento di Fisica e Scienze della Terra, Università degli Studi di Ferrara, Via Saragat 1, 44100 Ferrara, Italy, bncglc@unife.it

*corresponding author

Abstract

The F'Kirina plain in eastern Algeria is an endorheic basin suffering water scarcity due to a combination of natural and man-made causes. Its hydrogeological system is complex as made by interconnected aquifers represented by Mesozoic, Cenozoic, and Quaternary lithological units. The combination of drought indicators and water level data shows that a groundwater drought affected the plain during the last 15 years, which reflects on current water quality. The reported geochemical analyses, including major ions and trace elements, indicate that the groundwater resource is suffering from salinization, mainly due to evaporation and leaching of soil salts, a process that is coupled with simultaneous cation-exchange effects. In this framework, we observe a geochemical evolution from the fresh Ca-HCO_3 facies, typical of springs bordering the plain, towards more saline groundwater characterized by chloride/sulphate-rich facies in the middle of the plain approaching the sebka. However, geochemical diagrams indicate that in few wells salinization is also influenced by upraising of deep groundwater. The water isotopic composition of the F'Kirina plain samples suggests that they diversely record both recharge and evaporation components. Moreover, the most ^{18}O and D depleted compositions among the investigated ground-waters suggest recharge contributions by comparatively higher elevation or the involvement of old (fossil) water components.

Keywords
Groundwater salinization; Geochemical tracers; Stable isotopes; Drought; Water scarcity; Endorheic basin

1. Introduction

Water resources in the arid and semi-arid regions of the world are characterized by scarcity and high spatial and temporal variability. In these regions, with population growth, expansion of irrigated areas, and climate change, there is an increasing groundwater demand, which is the major source of water for drinking, irrigation, and industrial uses (UNESCO 2020).

North Africa, including Algeria, is considered a “climate change hotspot” (Diffenbaugh and Giorgi 2012) with a high year-to-year variability of rainfall amounts, drought periods, and heat waves (Cook et al. 2016; Lelieveld et al. 2016, Lionello 2012; Mariotti et al. 2015). Many projections and models estimate for the investigated area (and surroundings) a total annual precipitation decrease of 15-30% by the end of the twenty-first century (Christensen et al. 2007; Hadour et al. (2020) and that droughts will become more frequent and severe than those already observed during the 20th century (Reiser and Kutiel, 2011; Sousa et al., 2011; Hoerling et al., 2012; IPCC, 2013; Schilling et al., 2012; Zeroul et al., 2019).

Consequently, serious questions arise about the future agricultural practices, food safety, and local population displacement in Algeria and surrounding areas in the Middle East and North Africa (MENA) region (Alboghdady and El-Hendawy, 2016).

On this framework, other researchers focusing attention on water scarcity in the MENA region emphasized that water over-exploitation is aggravating the climatic effects (Haddadin, 2001; Leduc et al., 2017). Indeed, in semi-arid and arid regions of North Africa, long-term and large-scale exploitation of groundwater have significantly contributed to the deterioration of aquifers, with groundwater level decline (Bouchaou et al., 2011) and concurrent salinization, leading to the deterioration of the groundwater-dependent ecosystems.

Salinization often originates from a combination of natural and human factors, including seawater intrusion, dissolution of evaporite minerals (Bouchaou et al 2008; Re et al., 2014), mixing with deep saline waters/brines and geothermal fluids, cycling wetting and drying, and agricultural practices (irrigation and use of fertilizers). Seawater intrusion (accompanied by water-rock interaction) is often the main mechanism controlling groundwater salinization in North African coastal aquifers, as in Jerba Island (Tunisia, Souid et al., 2020) or Korba coastal plain (Tunisia, Zghibi et al., 2013); however, this is not the case of the F’Kirina inland aquifer. It is important to note that salinization affects also North Africa’s inland aquifers far from coastal zones. In this framework, salinization is mainly due to the dissolution of evaporite salts, as observed in several North African inland aquifers and endorheic basins (Farid et al., 2015; Mejri et al., 2018; Bouragba et al., 2011; Zereg et al 2018; Aouidane and Belhamra 2017).

Many inland basins in North Africa are characterized by the presence of chotts and sebkhas that form as salt pans, playa systems, and saline ephemeral lakes on low-laying and internally drained areas because of the local topography and the prevailing desert conditions. Information on saline waters contained in the chotts located in eastern Algeria comes from studies by Merzouk et al (2020) on Sahara lithium resources. The authors described that the surface of chotts is composed of halite and gypsum crusts, clastic muds, and very fine aeolian powder. The chott water levels mainly depend on the complex interplay between groundwater and surface water recharge, and subsequent evaporation. Coherently, the chott waters are often brines, where the effect of evaporation seems stronger than that of dilution by recharge from aquifers and precipitation; the main source of major ions is the dissolution of salts such as halite, epsomite, and gypsum. Chotts have a role in conditioning the hydrogeology of concerned basins and the quality of groundwater; many authors emphasize Total Dissolved Solid (TDS) gradients towards chotts and sebkas, likely caused by salt dissolution (Belkhiri et al. 2012; Ghodbane et al., 2015; Aissa et al., 2017), and/or by groundwater evaporation from salt pans as described by Schulz et al., 2015.

Noteworthy, the available studies on groundwater salinization rely on isotope hydrology and/or geochemical methods to recognize groundwater origin, sources of salinization, and associated water-rock interaction processes.

In this light, our research concerning the groundwater resources of the F'Kirina plain (north-eastern Algeria; Fig. 1) addresses the problem of groundwater salinization based on new hydrogeological, geochemical, and isotope data on groundwater obtained during two surveys, in April 2018 and November 2019.

These data are interpreted considering the hydrogeological structure of the aquifer and climatic conditions and give clues on the origin of groundwater recharge, flow paths, and water-rock interactions. Results are finally discussed in terms of source(s) and processes of groundwater salinization.

2. Description of the study area

2.1. Geographical and geo-hydrogeological setting of the study area

The F'Kirina plain, extended over an area of 650 km², is located in the North-East part of Algeria (North Africa) at the midpoint between the Mediterranean Sea and the Sahara (Fig. 1). It is part of the Constantine high plain and belongs to the Gareat El Tarf basin that is an extensive endorheic depression with a mean elevation of 960 m above mean sea level (AMSL), surrounded by mountains whose summits exceed the 2000 m AMSL.

The southern and northern borders of the basin are marked by relatively steep slopes as a consequence of the tectonic activity, which affected the region. The existing streams (Nini wadi, Ouelmene wadi, and Isfer wadi) flow toward depressions such as the Chott Gareat El Tarf, which is partially dry and salt-encrusted. This Chott is a protected wetland classified as Ramsar site and merges with other minor chotts located westward during major floods.

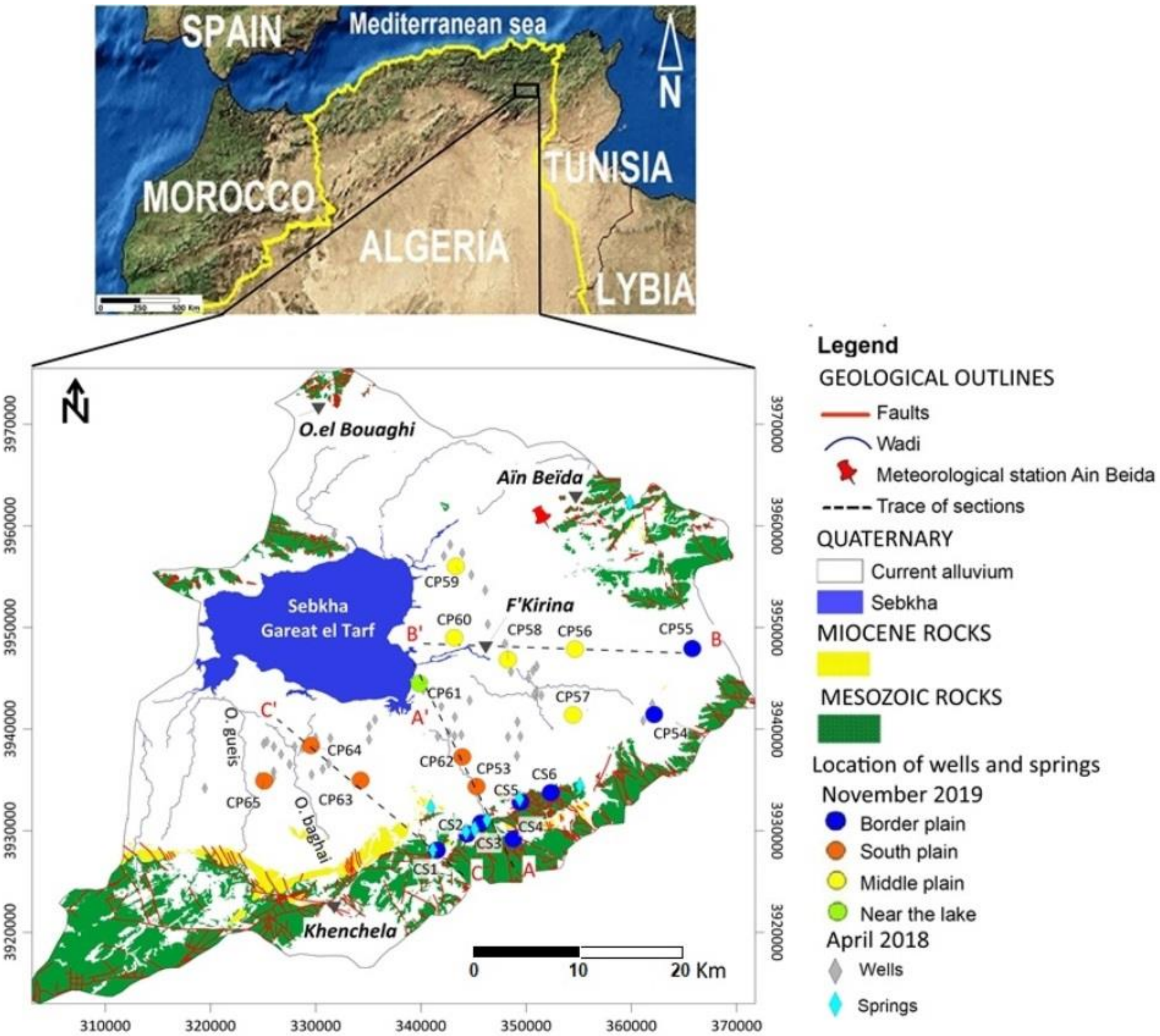

Fig. 1. Geological schematic map of F'Kirina plain, including the location of April 2018 and November 2019 sampling points; the latter are distinguished by geographical zonation (Coordinate Reference System: Datum World Geodetic System 1984, WGS 84, UTM ZONE 32N)

The geology of the Gareat El Tarf basin (which includes the F'Kirina plain) has been described by Voute (1967), Vila (1977), Guiraud (1977), and Benazzouz (1986). The stratigraphic series ranges from the Triassic to the Quaternary (Wilidi 1983). Formations of Mesozoic and Cenozoic age locate to the extreme East, North-East and South of F'Kirina plain (Fig. 1). The area characterized by Mesozoic rocks includes formations from Triassic to Upper Cretaceous. The latter form the backbone of the region: they are roughly oriented SW-NE and are largely formed by limestone and marl. Cenozoic (mainly Mio-Pliocene) formations characterise the middle and the south plain, where Quaternary formations also outcrop. The Sebkha of Gareat El Tarf is marked by Triassic outcrops, Miocene conglomerates, and by Quaternary deposits. The silty and clayey soil, impregnated by salts, is of low permeability.

The structures and landforms are the results of the two main Tertiary orogenic phases that are the Atlasic phase of Middle–Late Eocene age and subsequent Alpine Miocene phase (Laffitte 1939; Durosoy 1956). The Atlasic phase gave rise to large SW-NE and ENE-WSW folds, which were reactivated during the post-Miocene phases producing NW-SE and NE-SW faults (Guellal and Vila, 1973). The Miocene sediments lay on erosion surfaces thus forming a series of sometimes very deep depressions (Laffitte, 1939; Marmi, 1995). During Late Quaternary, E-W to NE–SW striking folds and reverse faults affected the young Quaternary deposits (Harbi et al, 1999). In particular, a syncline with younger Cenozoic rocks in inner parts and older Mesozoic rocks at the periphery is observed in the studied area.

From the hydrological point of view, the Lower Maastrichtian marly substratum outcropping at the border of the plain constitutes an impermeable base that is overlaid by permeable lithologies. The former includes the Maastrichtian fractured and karstified limestone outcropping to the East (whose thickness should not exceed 250 m) and the coarse Tortonian (Miocene) sandstones; the limestone of the Upper Maastrichtian constitutes the deep aquifer for the F'Kirina plain. The shallower hydrogeological structure corresponds to alluvial heterogeneous sediments (Mio-Plio-Quaternary) of variable permeability having in the whole a thickness of more than 300 m (Younsi, 2009). The above hydrogeological elements are synthesised in the schematic E-W geological section of Fig. 2. The main aquifer within this structure, which constitutes the most important source of groundwater for the area, is the Plio-Quaternary aquifer, with a large horizontal extension and a thickness from 10 to 100 meters, characterized by a succession of heterogeneous fluvial-lacustrine sediments composed of alternating gravels and clays, calcareous gravels, and pebbles.

The heterogeneity of the Plio-Quaternary lithology gives origin to a multi-layered aquifer system. Technical sheets of drillings (courtesy of Dept. of Water Resources, Wilaya of Khenchela) highlight a succession of saturated levels; local disconnection of aquifer levels is due to lenses of clays and marls, often with poor lateral continuity. However, the vertical hydraulic connection among saturated layers may naturally occur.

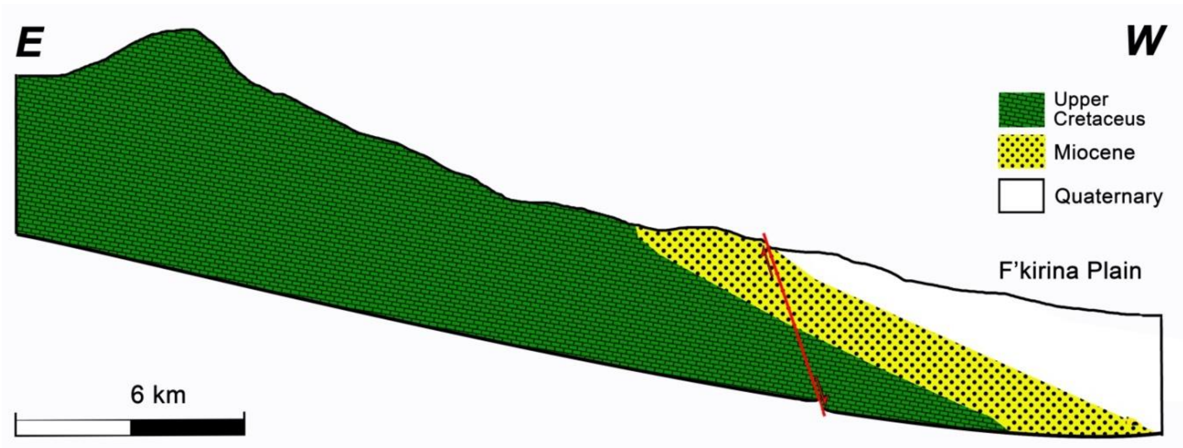

Fig. 2. Schematic E-W geological section

The Plio-Quaternary aquifer, beside a direct and local recharge from precipitation, receives a contribution from the Maastrichtian (Cretaceous) fractured and karstified limestone aquifers outcropping to the East and possibly from the Aures massifs to the South.

3. Material and methods

3.1 Precipitation data and groundwater level series

The study considers monthly average precipitation and temperature series measured in the period 1987-2020 at the rain gauge station of Ain Beida, located to the northern border of F'Kirina plain (Fig.1) (courtesy of National Meteorological Office of Ain Beida, Oum el-Bouaghi, Algeria). Data has been elaborated to calculate the meteorological drought indicators SPI (Standardized Precipitation Index, McKee et al. 1993) and SPEI (Standard

Precipitation-Evapotranspiration Index; McKee et al., 1993; Guttman, 1999; Lloyd-Hughes and Saunders, 2002; Vicente-Serrano et al., 2010; Beguería et al., 2014) at 12-month scale, which reflects medium-term precipitation patterns, thus being of hydrological significance (Potop et al 2012, 2014).
Time trends of the SPI and SPEI indicators have been compared to those of historical water level data (period 2003-2018) collected about every six months during low and high water periods by the Agence Nationale des Ressources Hydriques (ANRH) of Constantine (Algeria) on a monitoring network of 21 wells located in the F'Kirina plain. Measures were made with conventional hand-held devices.

3.2 Field surveys and sampling point technical data

The first survey concerning water level measure was carried out in April 2018 on a net of 73 wells (location in Fig. 4). On the same date, water sampling for preliminary (major element) analysis was carried out at 55 out of 73 wells and at 9 springs (Fig. 1). The investigation was repeated in November 2019, selecting 13 wells and 6 springs (location in Fig. 1) for a more complete geochemical investigation, which is presented in this paper. Most of the wells involved be the November 2019 sampling survey are located along the sections AA', BB' and CC' (Fig. 1).
Geographical and technical data of sampling points of this survey are in Tables 1S and 2S (Supplementary material). Water samples are grouped according to their geographical position as belonging to *i)* Border Plain (2 wells and 6 springs located at the highest elevation between 912 and 1282 m AMSL), *ii)* South plain (5 wells), *iii)* Middle plain (5 wells), and *iv)* Near the lake (1 well). The use of ground-waters from wells is both for domestic and irrigation purposes, while the main use of spring waters is domestic.
The considered wells are mainly drilled, with a mean depth of 107 m below ground (b.g.). Wells use shallow tube well technology, combined with small engine-driven pumps; although there is no information about the depth reached by tubes, the length of wells (Table 2S, Supplementary Material) indicates that they roughly cross the whole thickness of the Plio-Quaternary lithologies.
Most well technical sheets indicate a succession of saturated levels, suggesting that groundwater samples drawn by pumping may collect groundwater from more than one aquifer level, thus giving potential "mixed" information concerning their quality.

3.3 Water sampling and geochemical analyses

Groundwater samples in both sampling surveys were taken after well purging for at least 20 minutes; then, pH, Temperature, and Electrical Conductivity (EC) were measured in situ on each sample, using Portable Analyser Kit (Hanna HI 9812-5). Samples were stored at 4°C. Alkalinity was measured within a day at the Laboratory of Sedimentary environment and mineral and water resources in eastern Algeria of Tebessa University (Algeria). Samples collected in April 2018 were analysed at the same laboratory for a preliminary characterization concerning the major ions composition. Ca^{2+}, Mg^{2+} were analysed by atomic absorption spectroscopy using an Analyst 400 (Perkin Elmer), and Na^+ and K^+ with flame photometer model 410 (Sherwood); the volumetric method was used for bicarbonates and chlorides, while the spectrophotometer DR2000 (Hach) was used for sulphates. The average error balance for the 2018 samples is 1.3%.
Samples collected in November 2019 were analysed in Italian laboratories for a detailed investigation including minor and trace elements as well as oxygen and hydrogen isotopes. Anions (F^-, Cl^-, Br^-, NO_3^-, SO_4^{-2}) were analysed at the Department of Physics and Earth Sciences of the University of Ferrara (Italy) by ion chromatography using a Dionex

ICS-1000. Cations (Ca^{2+}, Mg^{2+}, Na^+, K^+) were analysed by ion chromatography using Metrohm IC-900 at the Department of Land, Environment, Agriculture, and Forestry of the University of Padova (Italy). The dissolved silica concentration (SiO_2 in mg/L) was determined using the Silica Portable Photometer HI-96705 (Hanna Instrument) that works in the range 0-2 mg/L. The average error balance is -2.3%.
Trace elements were analysed through an Agilent 7800 ICP-MS at the Department of Earth Sciences of the University of Florence (Italy) using Rh as internal standard, the Agilent Technologies tune solution containing 1 µg/L of Ce, Co, Li, Mg, Y in 2% HNO_3 matrix, and the Merck VI multi-elemental standard solution for calibration. Samples have been analysed at different dilutions to match the calibration range for most elements. Accuracy and precision, calculated on the basis of repeated analyses of samples and standards, were better than 10 % for all the considered parameters.
Hydrogen and oxygen isotopic composition was determined at the Physics and Earth Sciences Department of the University of Ferrara, using the CRDS Los Gatos LWIA 24-d isotopic analyser (Los Gatos Research). The isotopic ratios of $D/^1H$ and $^{18}O/^{16}O$ were expressed as δ notation ($\delta = (R_{sample} / R_{standard} - 1) \times 1000$) to the Vienna Standard Mean Ocean Water (V-SMOW) international standard. Three bracketing standards were systematically run during the analytical sessions. These standards, obtained from the Los Gatos Research Company, were calibrated according to the international IAEA (International, Atomic Energy Agency) protocol. Analytical precision and accuracy, based on replicate analyses of standards, were better than 0.3% and 1.0% for $\delta^{18}O$ and δ^2H, respectively (Marchina et al., 2015; Natali et al., 2016). As indicated in Marchina et al. (2020), the average standard deviation of 366 samples is 0.7‰ for δD and 0.14‰ for $\delta^{18}O$. Regression lines calculated in the next sections are obtained by the Ordinary Least Squares (OLS) method, and no significant differences are observed adopting other regression methods (Marchina et al., 2020).

4. Results and discussion

4.1 Climatic and hydrogeological setting

The results of the SPI and SPEI calculation at 12-month scale are shown in Fig. 3a and 3b respectively. SPI and SPEI give a different evaluation of drought intensity, however highlighting the same periods as to their occurrence. For the following considerations, we will consider the SPEI index, considered more reliable than SPI in the light of the inclusion of temperature in the calculation. Table 1 shows, concerning the different SPEI categories of drought/wet severity, the number of months in the period 1987-2020, and the percentage of months in the two periods 1987-2003 and 2004-2020.
Both Fig. 3b and Table 1 indicate that in the period 2004-2020 compared to the 1987-2003 period, there has been a decrease in the percentage of moderate, severe, and extreme drought months as well as of extremely, severely and moderate wet months, with an increase of the percentage of “normal months”. In the whole period of analysis, 50.5% of months shows a SPEI< 0; the comparison between the two sub-periods indicates a decrease of the total number of months with SPEI<0 during 2004-2020. Thus, the F’Kirina plain has suffered from droughts much more in the past than in the more recent period. The SPEI values indicate that the years of sampling (2018 and 2019) are “normal”; however, they are preceded by a period of severe meteorological droughts (spring 2016-winter 2017). The only data useful to understand the reaction of F’Kirina plain groundwater to the succession of drought periods are those collected for the period 2003-2018 by the ANRH.

Fig. 3c shows the time series of 9 (location in Fig. 4) out of the 21 wells of the net because they are the only ones for which measurements are regular on a half-year basis. However, selected time-series cover the level range characterizing the eastern part of the study area. The considered time-trends show that, after the severe drought of the period 2000-2002, WLs were steadily increasing till the middle of 2005 under the influence of the wet period 2003-2005. Then, from this period onwards, WLs, under a sequence of normal periods, gradually lowered. They reached their lowest levels in January 2018 (last measure) after the severe drought period of 2015-2017: compared to the maximum levels measured in mid-2005, the WLs showed a decrease between 5 and 23 m. Other records (not included in Fig. 3c because discontinuous) showed that at the end of this drought period some wells were completely dry. The last drought period is followed by a low recharge period, which became moderately wet only at the end of 2020 (Fig. 3b).

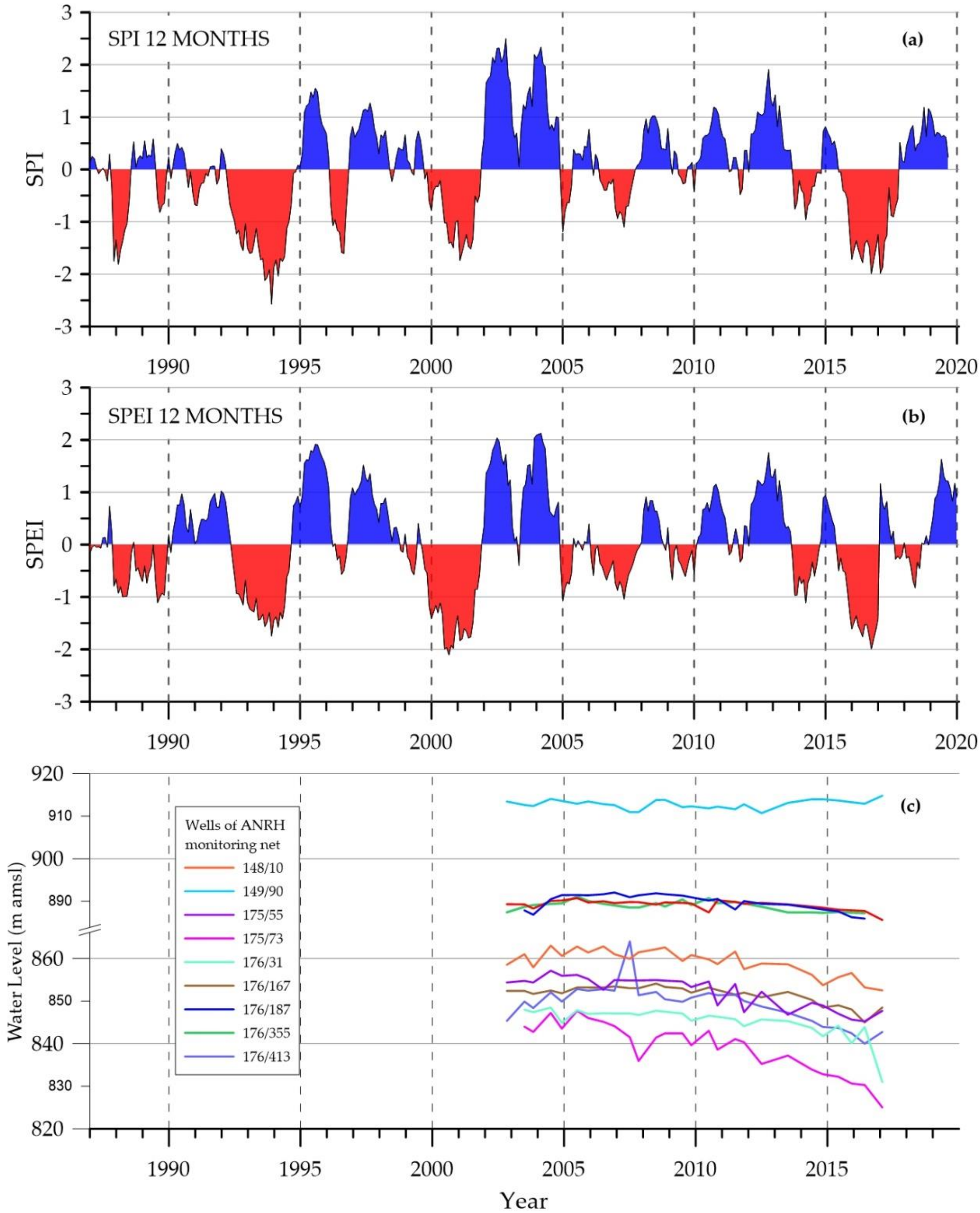

Fig. 3. SPI (a) and SPEI (b) calculated on a 12-month scale; (c) historical water level time-trends (ANRH, location of the wells in Fig. 4)

Table 1: Distribution (%) of different types of droughts according to SPEI

Period	% of months with SPEI < 0 on total months in the period
1987-2020	50.2
1987-2003	52.2
2004-2020	48.7

Categories of drought/wet severity	SPEI value	Number of months 1987-2020	Period 1987-2003	Period 2004-2020
			% of months/total months	% of months/total months
Extremely wet	SPEI ≥ 2	7	0.5	2.7
Severely wet	1.5≤ SPEI < 2	23	6	5.9
Moderate wet	1 ≤ SPEI < 1.5	53	11	8.9
Normal	-1 < SPEI <1	410	61.7	70.1
Moderate dry	-1.5 < SPEI ≤ -1	41	13.9	7.5
Severe drought	-2 < SPEI ≤ -1.5	18	5.9	4.9
Extreme drought	SPEI ≤ -2	4	1.5	0.5

The available data allow evaluating, the “groundwater drought” from 2005 till 2018, following the first severe drought period of 2000-2002. Groundwater droughts (with effects on groundwater quality and quantity) are consequent to meteorological droughts but are generally delayed compared to the onset of superficial effects of water depletion (Robins et al., 1997). Lags mainly depend on the severity and duration of meteorological droughts, their time sequence, physical characteristics of aquifers, and amount groundwater demand during rainfall breakdown. In the light of the above considerations and despite the low frequency of water level measures, we can conclude that both the investigated years 2018 and 2019 were under the effect of a long groundwater drought, with an influence on groundwater geochemical features.

The number of water level measures of April 2018 and the distribution of wells in the space was adequate to allow the elaboration of WL contour lines by Ordinary Kriging (Fig. 4). Water levels varied from more than 900 to less than 830 m AMSL, outlining a direction of groundwater flow from the recharge areas located in the eastern and southern mountains towards the Sebka of Gareat El Tarf. Water levels measured in October 2019 varied in the same range as those of April 2018, but either the number or the spatial distribution of prospected wells do not allow for meaningful geostatistical processing.

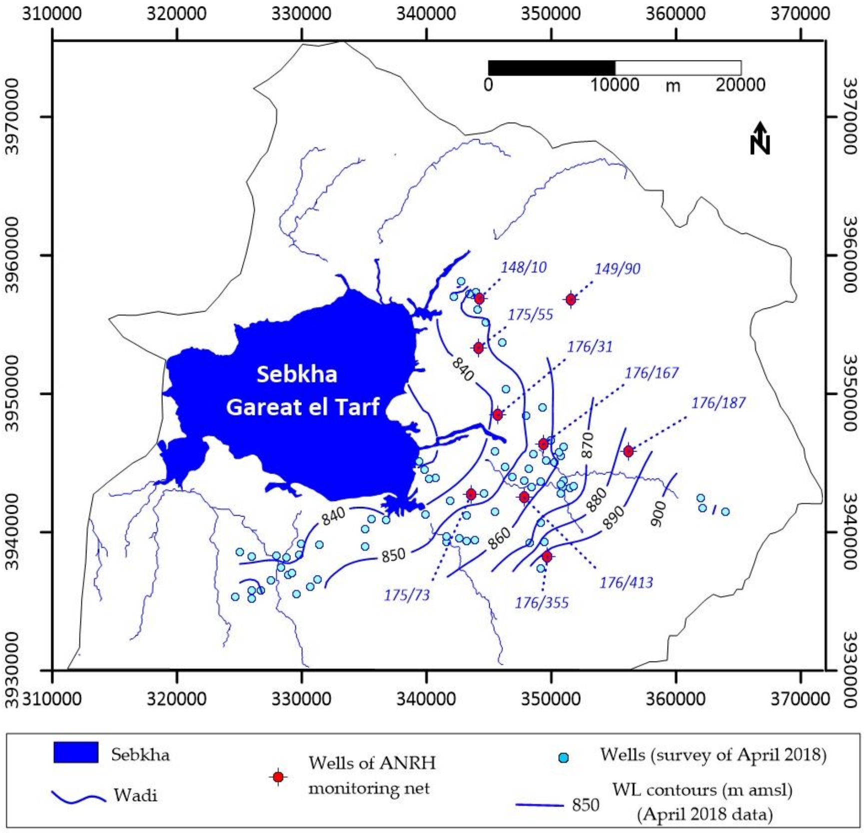

Fig. 4. Water level (WL) contours line of April 2018; location of wells of the ANRH monitoring net

4.2 Geochemical characterization of the studied waters

The data relating to groundwater and spring samples collected in November 2019 are discussed given their geographical zonation (Fig. 1); they are compared to data concerning the 2018 samples only for major elements. The whole data-set is commented in the light of the previously described hydrogeological and conceptual information. Analytical results of the 2019 survey, including the physicochemical measurements carried out in the field and the geochemical analyses, are reported in Table 3S (Supplementary material).
Preliminary statistical treatment of the 2019 analytical results has been obtained through a cluster analysis (dendrogram in Fig. 1S, Supplementary Material); the hierarchical relationship between samples highlights a link between the spatial distribution and the geochemical features, with some outliers (e.g. CP57, and in the minor extent CP53) that are quite different from the main group of samples. Results also show that some tracers such as chloride, bromide, sulphate, and sodium appear well correlated (R^2> 0.7, see the correlation plot in Fig. 2S, Supplementary Material) showing that their concentration is regulated by common dissolution and/or water-rock interaction processes.
The content in Total Dissolved Solids (TDS) of the 2018 groundwater samples varies between 397 and 2,491 mg/L, with an average of 933 mg/L, while spring waters show a TDS varying between 375 and 3,146 mg/L, with an average of 1,016 mg/L. As concerns the groundwater samples of the 2019 survey, those of the plain show a TDS between 337 and 4,701 mg/L, with an average value of 1,473 mg/L, while the TDS of the spring waters collected at the border plain varies between 303 and 466 mg/L, averaging 378 mg/L. TDS values higher than 1,500 mg/L relate to CP65 and CP63 samples in the South plain, to

those collected in the Middle plain (CP58, CP59, CP60, and CP57), and Near the lake (CP61).

Water samples of both sampling survey have been classified (Fig. 5) using the Hydrochemical Facies Evolution diagram (HFE-D, Giménez-Forcada, 2010; Giménez-Forcada and Sánchez San Román, 2015). In this diagram, hydrochemical facies (HF) are determined as a function of calcium and sodium (cations) percentages, and bicarbonate and chloride (anions) percentage to the sum of cations and anions, respectively.

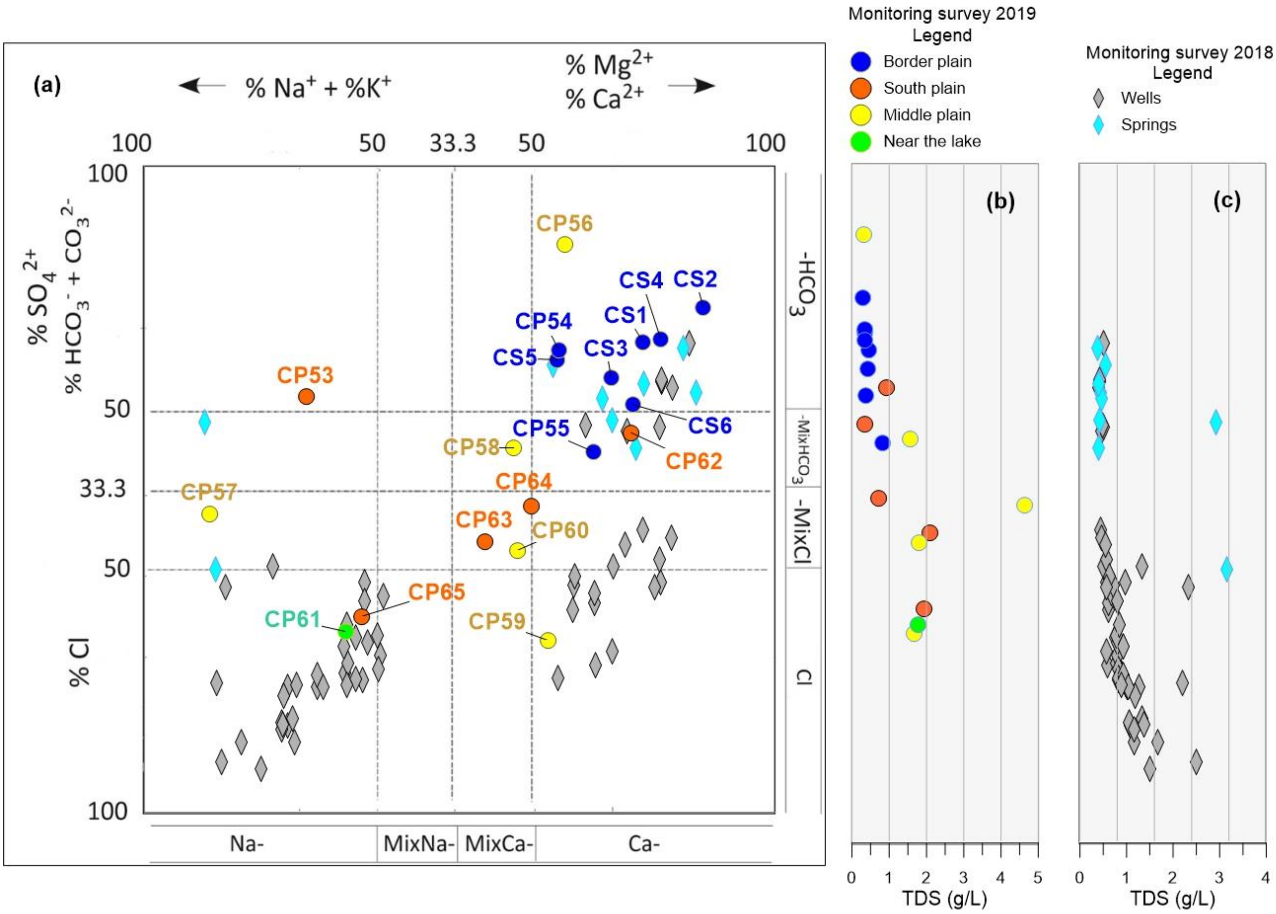

Fig. 5. a) HFE diagram of the studied waters; b) and c) TDS variation of the 2019 samples and 2018 groundwaters and spring waters respectively, corresponding to HF evolution. The 2019 samples are distinguished by their code and marked according to geographical zonation (Fig.1).

The diagram includes four main "heterotopic" facies (Na-HCO_3, Na-Cl, Ca-HCO_3, and Ca-Cl), which are defined by cation and anion percentages higher than 50%. When a facies includes the Mix term coupled to a cation or an anion or both ions (hybrid facies), this indicates that the percentage of the cation or anion is less than 50%, but, at the same time, it is the highest percentage compared to the other considered cations and anions. The abscissae, which separately represent the percentages of Na^+ and Ca^{2+} in meq/L, reproduce the base-exchange reactions: thus, the HFE-D is particularly effective in the description of heterotopic (as Na-HCO_3 and Ca-Cl) and hybrid HFs often occurring when mixing of distinct groundwater end-members triggers cation-exchange processes. The percentages of anions are in the ordinates, where the percentage of chloride is connected to groundwater salinization due to seawater or chloride-salts and the percentage of bicarbonate or sulphate (depending on the dominant anion in freshwater) characterizes recharge waters. Fig. 5 integrates a plot showing for each HF the corresponding TDS (Giménez-Forcada, 2018). The diagram allows outlining water evolution within the aquifer.

The HF Ca-HCO_3 marks the 2019 springs, the samples CP54 and CP56, and some springs and wells of the 2018 survey. These pristine waters evolve to CaMixHCO_3 type (CP62, CP55, and other springs and wells of the 2018 survey) with TDS increase. Further increase in TDS leads to hybrid HFs such as MixCaMixCl (CP60, CP63, CP64) and MixCaMixSO_4 (CP58); then hydrochemical facies as NaCl appear in the Middle plain (CP65) and Near the lake (CP61), maybe indicating dissolution of chloride (and sulphate) salts; this HF also marks most of the samples of the 2018 survey. The remaining 2019 samples follow different evolution paths: the CP53 and CP57 samples show the Na-HCO_3 and NaMixCl facies, respectively, while the sample CP59 shows the Ca-Cl facies (as many of 2018 samples). The genesis of these last HF types of groundwater is not straightforward and can be related to various factors. The HF of CP53, which is quite fresh (0.9 g/L), can be the proxy of a deep fresh end-member circulating in rocks including Na-rich ion-exchangers (clay), where a slow equilibration of freshwater with the exchange complex causes a series of reactions that favour the sequential release of Mg^{2+} and Na^{+} to the solution in exchange for Ca^{2+}. The concurrent increase in a closed environment of total alkalinity ad Na^{+} could be related to the availability of calcite, which dissolution is triggered by the under-saturation induced by the loss of dissolved Ca^{2+} subtracted by cation exchange. This process implies that Na^{+} amounts in the exchangers are much higher than those of Ca^{2+} carried by freshwater, resulting in a very high ratio of adsorbed ions/ions in solution: the succession of the different hydrochemical facies during this process of softening is, therefore, a rather slow process (Lambrakis and Kallergis, 2001), since it requires the passage of a volume of freshwater contributing Ca^{2+} in relatively low concentration many times greater than the volume of the pores to move all the Na^{+} from the exchange sites.

The CaCl facies of CP59 likely originates from the inverse exchange Na/Ca: such type of facies is normally observed during active seawater intrusion on coastal aquifers where clay sediments in equilibrium with freshwater are flushed by saline waters (Appelo and Willemsen 1987; Beekman 1991). Same HFs can be originated in continental aquifers in connection to groundwater salinization by the dissolution of salts.

The CP57 (with a TDS of 4.7 g/L) shows a NaMixCl HF; however, it has a high content of bicarbonates (1500 mg/L) with a percentage barely smaller (24.6%) than that of chlorides (25.6%). CP57 positions along an evolution path in between two springs (named Elkenif and Gaarir) sampled during the 2018 survey: these springs are marked by NaCl, and NaMixSO_4 HFs, and a TDS of 3.1 and 2.9 g/L, respectively. Both springs are thermal springs used from the Roman time as Spa. They show high temperatures at the outlet (46 and 38°C). This analogy shows that salinization in the area is not linked only to evaporation and leaching of Quaternary salty deposits at shallow levels but, at least in few cases, can be inherited also by deeper contributions outpouring from the basal levels of the Mesozoic rocks.

Thus, F'Kirina groundwater may be subject to different processes, according to the aquifer lithology, as ion exchange and dissolution of salts. For comparison, we report variations in salt content and facies shown by other researchers who studied the F'Kirina plain in the last years. Dib et al. (2017) analysed 47 samples (unknown sampling date), classified in F'Kirina and Ain Zitoune groups, which roughly correspond to the Middle and South Plain groups of our study. The EC of ground-waters of F'Kirina group is between 550 and 6060 μS/cm, while the EC of samples of the Ain Zitoune group varies in the range 600-15,800 μS/Cm. The dominant HFs are CaMgSO_4Cl and CaHCO_3. Dib et al. (2017) attributed the significant correlation (r^2> 0.8) between sodium, chlorides, and sulphates to widespread evaporation processes. Salima and Belgacem (2017) analysed 45 samples (May 2015) in an area corresponding to the Middle Plain. The EC ranges from 220 to 6,700 μS/cm, while HFs vary from CaHCO_3 to CaSO_4 in the Plio-Quaternary sediments; CaCl facies are found near the Sebkha. In November 2016 Kahal et al. (2018) analysed 21 groundwater samples in an area corresponding to the Middle Plain; they found predominant $CaSO_4$, $CaHCO_3$, and CaCl facies; there are no data on EC and TDS. These findings suggest that water quality in the F'Kirina plain is highly variable, depending on the selected well net, and survey season and year.

Figs 6a and 6b show the relationships between Na and Cl and (Ca+Mg) vs (HCO_3+SO_4) respectively. The Na/Cl ratios are generally lower than 1 both for springs and groundwater (Fig. 6a), with few exceptions such as the two thermal springs of 2018 sampling, and the CP53 and CP57 samples that show Na/Cl ratio higher than 1.

Spring waters mostly lie on the 1:1 line in Fig. 6b, indicating that calcium and magnesium originate from the dissolution of calcite, dolomite, and gypsum/anhydrite. Downstream groundwater, if compared to the 1:1 line, shows either excess (CP57, CP53, and some springs of 2018 sampling) or depletion of sulphate and bicarbonate. The former are Na-HCO_3 and NaMixCl, NaCl, and NaMixSO_4 waters respectively, while the latter (that also show Na/Cl ratio lower than 1) could be associated with the effects of dissolution of halite followed by inverse ion exchange, with calcium and/or magnesium increase and sodium depletion (Fig. 7a).

On the contrary, CP53 and CP57 HFs indicate a direct ion-exchange (Na increase and calcium and magnesium depletion) leading to Na enrichment. This means that the leaching of evaporite minerals such as halite, gypsum, carbonates, natron, and trona, typically observed in Algerian chotts (Zatout et al., 2020) is coupled with significant cation exchange processes in which Na is exchanged with Ca and vicariant elements.

Fig. 7b shows the relationship between the HCO_3/(SO_4+Cl) ratio and EC; it confirms that the EC increase from the left (carbonate pole) towards the right (evaporite pole) is mostly due to the increase of both chlorides and sulphates. The samples related to CP53 (Na-HCO_3), CP57 (NaMixCl), two thermal springs (NaCl and NaMixSO_4), and CP59 (CaCl) deviate from the general trend because of the overlap of cation-exchange (direct or inverse).

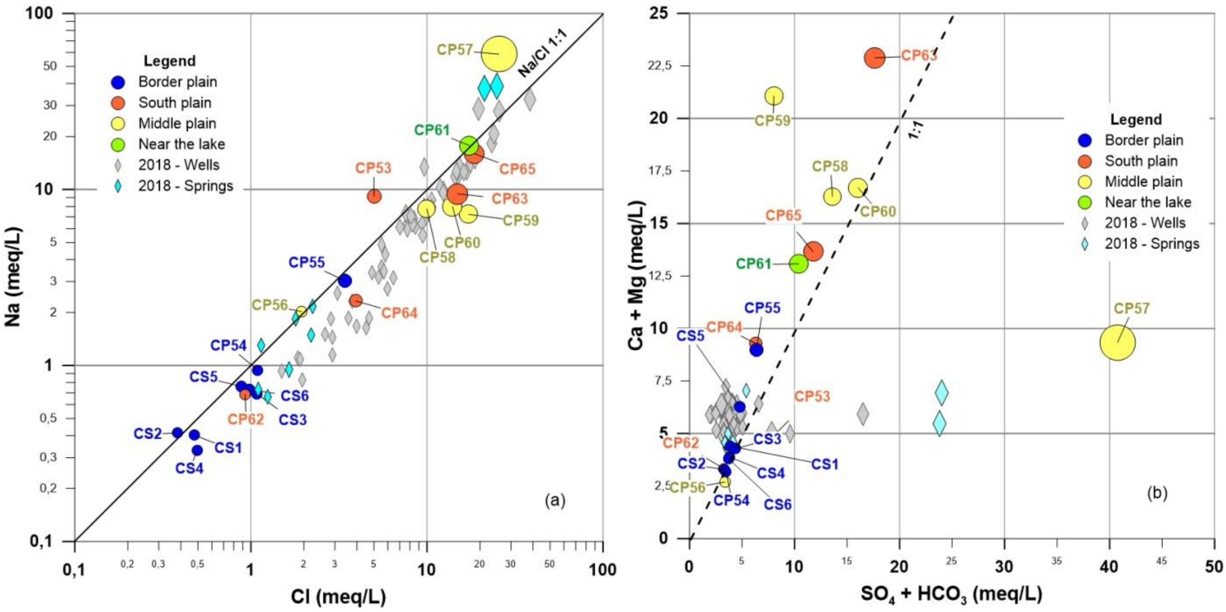

Fig. 6. (a) Relationship between Na and Cl concentrations; (b) Relationship between Ca+Mg and SO_4+HCO_3 concentrations. In both graphs, the symbol size is proportional to TDS.

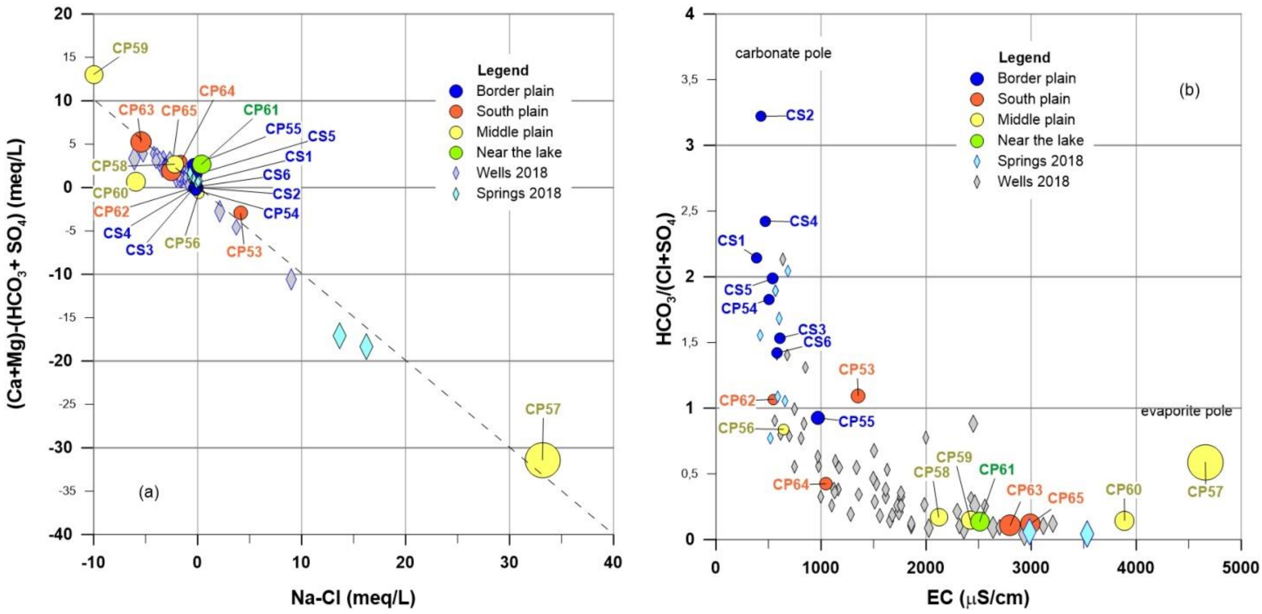

Fig. 7. a) Relationship between the (Ca+Mg)-(HCO_3+SO_4) difference and the Na/Cl ratio; (b) relationship between the HCO_3/(SO_4+Cl) ratio and EC. The symbol size is proportional to TDS.

Fig. 8 shows the relationship between the Cl/Br (molar) ratio and chlorides. The Cl/Br ratios of the low salinity springs should reflect the ratio of the local rainfall. Evaporation of infiltrating water increases the chloride concentration in recharge waters, but leaves Cl/Br unaffected: thus recharge by direct rainfall infiltration with subsequent evaporation seems to interest most of the ground-waters of the Middle plain. The most likely reason for the concurrent increase of Cl/Br ratios and salinity is the dissolution of halite that is contained in the local salty lithologies.

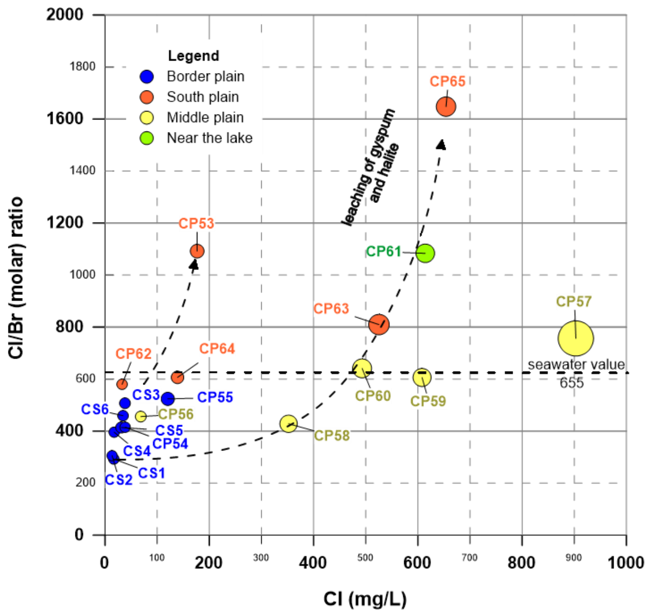

Fig. 8. Cl/Br (molar) ratio vs. chloride concentrations; the symbol size is proportional to TDS.

Lithium (Fig. 3Sa, Supplementary Material) and Boron (Fig. 3Sb, Supplementary Material) tend to increase, although not systematically, in parallel with the Cl/Br, suggesting that boron minerals (borax, colemanite, ulexite; Helvaci and Palmer, 2017) and lithium minerals

(Li-rich phyllosilicates, Mertineit and Schramm, 2019; Bekele and Schmerold, 2020; Zatout et al., 2020) are locally present in the salt pans and can be leached; then a simultaneous cation exchange occurs (Abdelkader et al., 2012; Demdoum et al., 2015).

Among trace elements that can vicariate calcium, Sr (probably hosted in sulphates and carbonates) is preferentially released compared to Ba in parallel with salinization, as demonstrated by the positive correlation between the Cl/Br and Sr/Ba ratios (Fig. 4S).

Most of the Cl/Br ratios below seawater value are associated with medium and high nitrate concentrations. Fig. 5Sa (Supplementary Material) indicates possible localized groundwater pollution caused by the use of Br-based pesticides in agriculture and leaching of septic waste (Alcalá and Custodio 2008). CP53 and CP61 show nitrate concentrations lower than those found in the springs, close to background levels.

Fig. 5Sb (Supplementary material) shows the relationship between NO_3 and TDS. Two main groups can be distinguished in the more saline waters: (A) with high nitrate contents and (B) with low nitrate contents. As to Group A, nitrate concentrations indicate input from irrigation return flows containing nitrogen compounds: CP63 and CP65 also show high Cl/Br ratios. Group B shows nitrate concentrations less than 40 mg/L, more likely influenced by septic tanks leaching. In this view, it is important to emphasize that recent studies in salty environments demonstrated that nitrogen retention is microbially mediated and can be stocked and released (Yang et al., 2015).

Fortunately, salinization and related cation exchange processes do not release in groundwater toxic heavy metals such as Ni, Co, Cr, V, Cu, Zn, Pb, As, and U (Table 4S, Supplementary Material) that often are below the detection limits and always below common WHO thresholds defined for drinking water.

4.3 Isotopic composition of the studied waters

Oxygen and hydrogen isotopes were also measured for groundwater and spring in the F'Kirina plain (Table 2). The waters have $\delta^{18}O$ that varies between -9.7 ‰ and -5.9 ‰, with an average value of -7.1‰, while δD varies between -61.3‰ and -40.3‰, with an average value of -50.1‰. The springs located at the border of the plain show a $\delta^{18}O$ ranging between –8.1‰ and -7.3‰ with an average value of -7.6‰, and a δD ranging between -49.1‰ and -45.1‰, with an average value of -47.8‰. Isotopic data are represented in the $\delta^{18}O$ - δD binary plot compared to the Global and Local Meteoric Lines (GMWL, Craig, 1961; Gat and Dansgaard, 1972).

The d-excess values were computed assessing potential evaporation effects (d-exc = $\delta D - 8*\delta^{18}O$, Dansgaard, 1964). Large variability is observed across the global and local scales. The Eastern Mediterranean (Gat and Dansgaard, 1972; Bowen and Revenaugh, 2003) shows values higher than 15, with a gradient of 6‰ from the Aegean Sea to the coast of Israel (Saighi, 2001). The meteoric line for the Eastern Mediterranean is estimated to be on average $\delta D = 8*\delta^{18}O+20$ (Saighi, 2001; Bowen and Revenaugh, 2003; Aouad-Rizk et al., 2005) while for the Western Mediterranean it is $\delta D = 8*\delta^{18}O+13.7$ (Celle-Jeanton et al., 2001). This reflects the difference of origin and the vapour supply and removal history of the air masses over the two areas, which is also observed in recent isotopic data of atmospheric vapour. In this study, the d-excess varies between 2.3‰ and 16.7‰ for groundwater and between 9.3‰ and 16.7‰ in the spring waters.

Table 2. Stable isotopes of the F'Kirina plain waters.

Sample code	δD (‰)	$\delta^{18}O$ (‰)	d-exc (‰)
Border plain			
CS1	-47.9	-7.6	12.9
CS2	-49.1	-7.3	9.3
CS3	-49.0	-7.4	10.2
CS4	-48.1	-8.1	16.7
CS5	-45.1	-7.5	14.9
CS6	-47.3	-7.8	15.1
CP54	-55.8	-7.8	6.6
CP55	-50.5	-6.9	4.5
Middle plain			
CP56	-55.2	-7.9	8.1
CP57	-50.6	-6.7	8.1
CP58	-49.7	-6.6	3.1
CP59	-49.5	-6.5	2.7
CP60	-42.2	-5.9	2.3
South plain			
CP53	-61.3	-9.7	16.7
CP62	-52.6	-7.7	8.9
CP63	-40.3	-6.1	8.6
CP64	-50.8	-7.5	9.0
CP65	-44.5	-6.7	9.0
Near the lake			
CP61	-49.0	-6.8	4.6

Fig. 9 shows the $\delta^{18}O$ - δD relationship of the sampled waters together with *i)* the Local Meteoric Water Line (LMWL) referred to isotope data of precipitation collected at USTHB University in Bab-Ezzouar (Algiers) between 2000-2004 ($\delta D = 7.15\ \delta^{18}O+7.92$, R^2 =0.9, n=113; Saighi 2005), *ii)* the Western Mediterranean Water Line (WMWL, $\delta D = 8*\delta^{18}O+13.7$, Celle-Jeantone et al 2001), and *iii)* the Global Meteoric Water Line (GMWL, $\delta D = 8.17*\delta^{18}O+10.35$, Rozanski et al 1993). Fig. 9 also shows the isotope stable composition of springs of high altitude emerging from Aures mountains, located to the south of F'Kirina plain (data from Belkoum et al 2020), and of waters from wadis and dams of Chemora area, which locates to the west of F'Kirina plain (data from Belkoum and Houha 2017). Springs of the Aures Mountains and springs of the Border plain group have been merged for reconstructing the F'Kirina spring line. The GW F'Kirina Plain line represents the Linear Regression Line of stable isotope data of the groundwater samples from the wells of the F'Kirina plain.

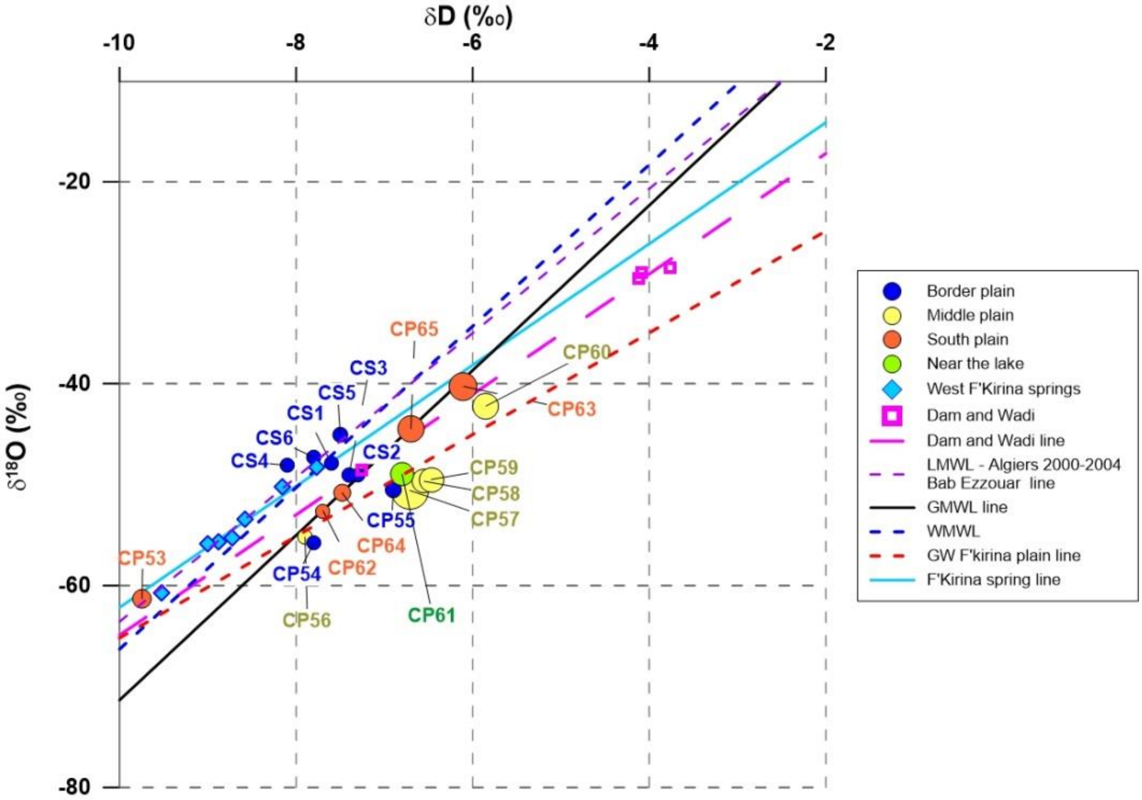

Fig. 9. $\delta^{18}O$ - $\delta^{2}D$ diagram concerning the groundwater (GW) and spring waters of the F'Kirina area. Symbol size is proportional to the TDS of samples.

Isotope data of sampled waters show a slight positive correlation (R^2=0.57, n. 19) with a regression line having a slope of 4.2, which is quite different compared to the slope of 8 related to the WMWL. The springs collected at the plain border are mostly located close to the WMWL and LMWL, indicating the possible contribution of local precipitation to the recharge. On the WMWL and LMWL, we also find the high elevation springs of the Aures massifs.

Most of the ground-waters of the plain are placed at the right of LMWL and GMWL. Their average d-excess, excluding the sample CP53 (d-excess 16.7‰), is 6.3‰: CP53 is the only groundwater sample placed close to the LMWL with more negative isotope values than those of both the springs of South and South-East mountains. If we exclude springs, the $\delta^{2}D$-$\delta^{18}O$ relationship of the only ground-waters from wells (F'Kirina GW line in Fig. 9) shows a good correlation (R^2=0.82, n. 13), with an equation having a slope of 5. The line related to waters from dams and wadis of the Chemora area follows a trend mostly parallel to the F'Kirina GW line.

Groundwater samples from wells are aligned along a regression line; this can be explained by taking into consideration that during evaporation processes the isotopic composition of the residual liquid gradually departs from the LMWL, following a nearly linear trajectory known as evaporation line (Gat and Gonfiantini, 1981; Gonfiantini 1986).

If we consider the intersection of the F'Kirina GW and LMWL lines, the resulting isotopic value is close to the CP53 signature ($\delta^{18}O$ -9.4‰ and δD -61.7‰), providing useful information to estimate the isotopic composition of the recharging waters (Gibson et al., 1993). The isotopic composition of this water plausibly represents a recharge from the high parts of the Aures Mountains, and/or the contribution of past precipitation, with different climatic conditions compared to the present time (Tarki et al., 2012; Demdoum et al., 2015; Mokadem et al., 2016). In other words, we assume that CP53 and the spring samples (that reflect the average isotopic composition of the current precipitation) are the end-members of the recharge process that variously mix to feed the groundwater system of the plain.

This framework is coherent with the $\delta^{18}O$ vs. electrical conductivity and $\delta^{18}O$ vs. elevation relationships observed in Figs. 10a and 10b respectively. In particular, Fig. 10a shows that when EC exceeds 2000 μS/cm the $\delta^{18}O$ values concurrently increase. Fig. 10b shows the relationship between $\delta^{18}O$ and elevation for springs emerging both from the Aures Mountains, located south of F'Kirina plain, and those belonging to the South-East mountain range. The regression of $\delta^{18}O$ vs. elevation data for the whole springs gives an altitude gradient of -0.27 $\delta^{18}O$/100 m.

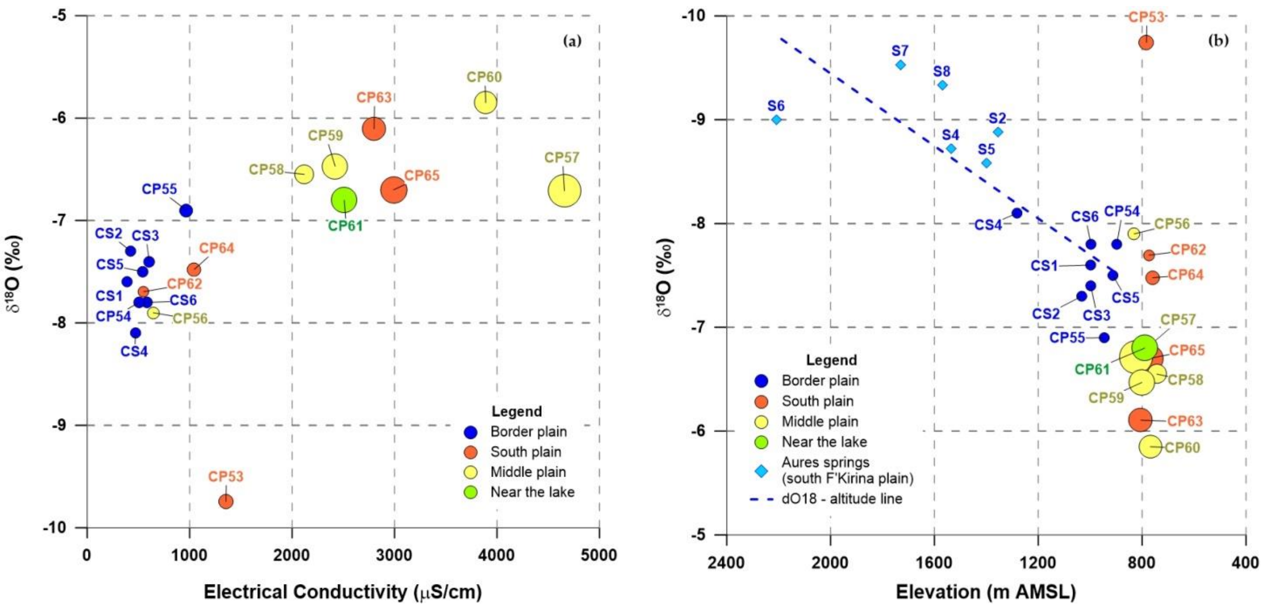

Fig. 10. (a) Relationship between $\delta^{18}O$ contents and EC; (b) Relationship between $\delta^{18}O$ and elevation of springs and well-heads. Symbol size is proportional to sample chloride concentrations.

It is also interesting to evaluate the stable isotope variation along some selected transects traced from the border of F'Kirina plain towards the lake (traces in Fig. 1). The transect AA' in Fig. 11 (with direction SSE-NNW) connects the springs CS4, CS2 and CS3, and the wells CP53, CP62 (South plain) and CP61 (Near the lake) (Table 2).

The $\delta^{18}O$ does not increase systematically towards the lake, while the water level in wells decreases; however, CP61 shows a higher water level than the upstream wells. CP53 does not connect with stable isotope data of the considered springs: in the light of Fig. 10b, its isotopic composition should refer to a recharge area at about 1700 m AMSL. CP62 too shows a depleted isotopic composition compared to the springs located along the AA' transect, while only CP61 has an isotopic composition similar to that of springs.

The transect BB' (with direction E-W, Fig. 11) intercepts the samples: CP55, CP56, CP58, and CP60. The $\delta^{18}O$ becomes less negative towards the lake going from CP55 to CP58, and CP60; however, CP56 is out of the trend, having more depleted isotopic values and a saline content lower than the upstream groundwater (CP55). CP60 shows both a higher water level and higher salinization than the upstream well. The transect CC' (directed SE-NW, Fig. 11) crosses CS1 spring and CP63, CP64, and CP65 wells.

Even here we observe that CP64 has isotope values lower than CP65 located upstream.

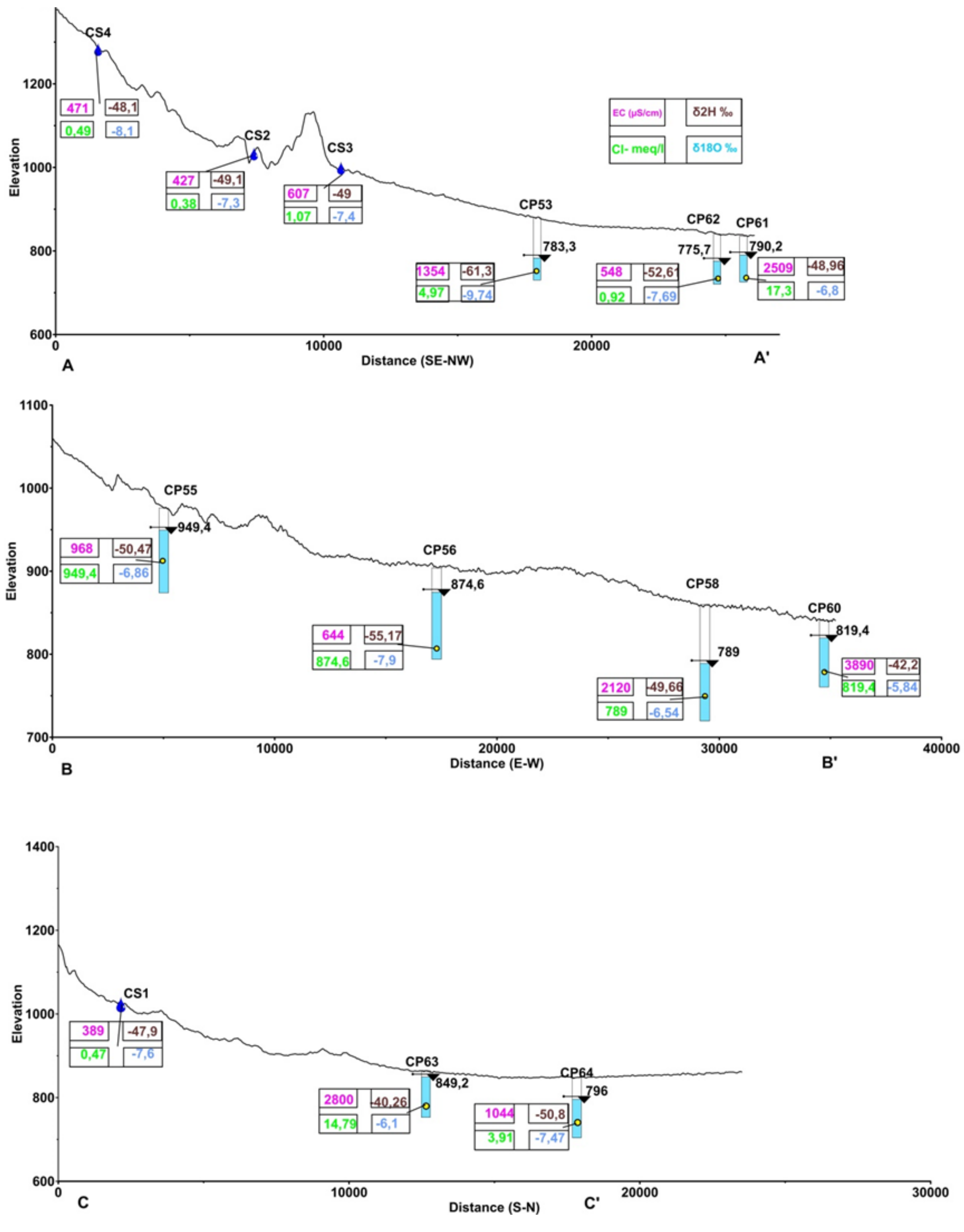

Fig. 11. Water level, geochemical and isotopic variation along the AA', BB' and CC' transects (traces in Fig. 1).

Taken together, isotope data along transects suggest that water samples do not represent groundwater of a unique aquifer. We should remind that sampled wells (whose equipment and position of pump is unknown) can intercept different saturated levels, locally disconnected by less permeable material; however, wells can interconnect saturated levels, giving a pumping sample with "mixed information", which is not easy to unravel. Besides this possible saturated level mixing due to well artefacts, we should also consider the contribution of return flow, which effects overlap those of the complexity of the aquifer saturated levels.

5. Conclusions

The hydrogeological system that feeds groundwater in the F'Kirina plain is complex as made by interconnected aquifers represented by Mesozoic, Cenozoic, and Quaternary. Piezometric investigation shows that a groundwater drought affected the F'Kirina plain during the last 15 years likely because of the concurrence of a meteorological drought succession and over-exploitation. Geochemical analyses indicate that the decreasing water resource is also suffering from general salinization, mainly due to evaporation and leaching of soil salts, a process that is coupled with simultaneous cation-exchange effects.

In this framework, we observe a general geochemical evolution from the fresh Ca-HCO_3 facies typical of springs bordering the plain towards more saline groundwater, characterized by chloride/sulphate-rich facies, which are found in wells in the middle of the plain, approaching the sebka. Uprising of deep saline groundwater, although subordinate, is also recorded as suggested by the site CP57 and the neighbouring thermal springs.

Coherently, the oxygen and hydrogen isotopic analyses plotted in the notional δ^2H-$\delta^{18}O$ diagram record distinct trends, spanning between the regression line defined by the local spring compositions, which reflects the characteristics of the water recharge components, and the regression line of groundwater in the plain, which records various degrees of evaporation.

Isotopic analyses also suggest that the F'Kirina plain ground waters incorporate far-field water contributions that, having comparatively more negative oxygen and hydrogen isotopic composition (δD-$\delta^{18}O$ down to -61.3‰ and -9.7‰, respectively), demonstrate either their origin from altitudes higher than those of the sampled springs (δD between -49.1‰ and -45.1‰, $\delta^{18}O$ between -8.1‰ and -7.3‰) or the drainage of old water components recharged under climatic conditions cooler than at present.

These statements are corroborated by the isotopic diagram of Fig. 12, where the F'Kirina plain groundwater composition is compared with that of groundwater of neighbouring regions where the fingerprint of distinct aquifers has been highlighted. It can be noted that F'Kirina plain groundwater mainly conforms to isotopic features of Upper Cretaceous aquifers that are an important reservoir at the regional scale. The unique sample having decidedly more depleted (negative) isotope ratios has been observed at the border of the plain, where the older rocks, which are included in the syncline system, outcrop. This composition recalls that typical of older aquifers that in surrounding areas are ascribed to the Lower Cretaceous (Abid et al., 2011; Tarki et al., 2012; Kamel, 2013; Mokadem et al., 2016). Deeper aquifers are generally characterized by more negative isotope composition inherited by palaeo-precipitation having δD-$\delta^{18}O$ lighter than the present-day weighted mean value for rain (Edmunds et al., 2003), possibly having Holocene (Abouelmagd et al., 2012) or even Late Pleistocene age (Guendouz and Moulla, 2010; Darling et al., 2018). However, the involvement of such deep and old water components cannot be assumed as the general source of salinization, which appears mainly to be related to water-rock interactions within the shallower (and salt-bearing) Miocene-Pliocene and Quaternary aquifers in the presence of concomitant evaporation.

The comparison of current results with those of other surveys carried out in the F'Kirina plain shows the existence of differences in groundwater chemical composition in distinct years. These differences may indicate that the aquifer system, in its most exploited part, has a flow connection of local or intermediate dimension, very sensitive to seasonal and inter-annual variations, while some hydrochemical facies, which seem unusual compared to the whole set, might be the expression of intermediate or regional flow systems (with a deeper circulation).

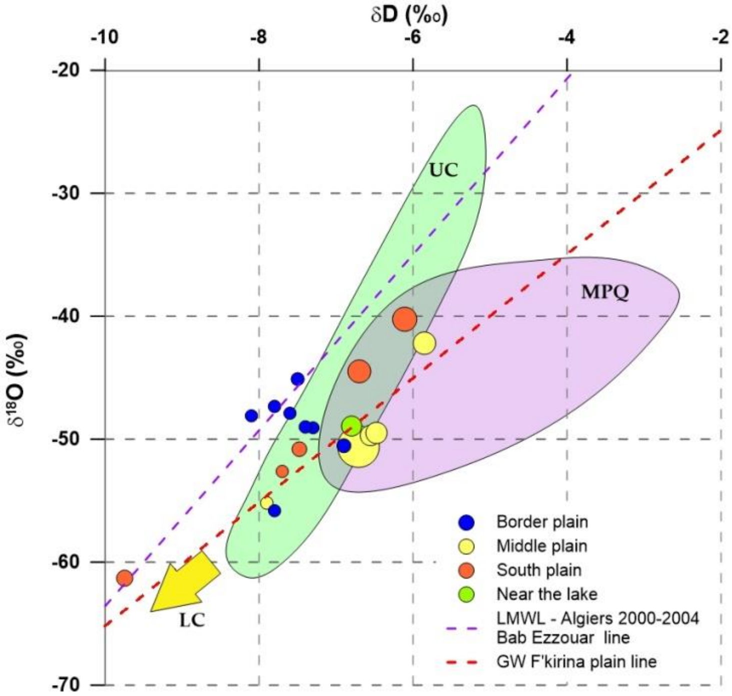

Fig. 12: Isotope composition of F'Kirina Plain waters compared to groundwater from Upper Cretaceous (UC), Lower Cretaceous (LC) and Miocene-Pliocene-Quaternary (MPQ) aquifers of surrounding localities. MPQ data from Tarki et al. (2012), Kamel et al. (2013) and Mokadem et al. (2016); UC data from Abid et al. (2011) and Mokadem et al. (2016); LC data from Abid et al. (2011) and Edmunds et al. (2003). GW is the regression line of F'Kirina area groundwater and the MWL is the local meteoric line of Algiers, as explained in section 4.5.

Besides diffuse salinization, water levels and their comparison with previous information related to the last decade, suggest a decrease in groundwater volumes. Under possible climate changes that ultimately may lead to an increase in drought periods and a concomitant increase of water demand, groundwater shortage and salinization may probably get worse. The data collected in November 2019 represent the updated snapshot of the current conditions. They can represent an essential benchmark for future monitoring, to understand how the on-going climatic changes affect the local water resources in terms of both quantity and quality. The information is fundamental to provide advice and best practices for local water management.

Author contribution

Conceptualization, R.O, M.D.F., G.L.; Methodology, M.C, N.C.; Investigation, R.O., G.L., M.C., N.C; Supervision, B.G., G.L., M.D.F., N.C.; Data collections, R.O.; Data curation, R.O, M.C., B.G., N.C., M.D.F.; Writing—Original Draft, R.O., M.C., M.D.F.; Writing—Review and Editing, B.G., N.C.. All authors have read and agreed to the published version of the manuscript.

Acknowledgements

This research was supported by the Algerian Ministry of Higher Education and Scientific Research (Programme PNE 2019-2020).

The authors are grateful to the Research Team of Politecnico di Bari involved in the PRIMA-MEDSAL Project (http://medsal.eu) for the support in the training of PhD student Omar Rahal.

Funding sources

This research did not receive any specific grant from funding agencies in the public, commercial, or not-for-profit sectors.

References

Abdelkader, R., Larbi, D., Rihab, H., Fethi, B., Chemseddine, F., Azzedine, H., 2012. Geochemical characterization of groundwater from shallow aquifer surrounding Fetzara Lake NE Algeria. Arab. J. Geosci. 5, 1–13. https://doi.org/10.1007/s12517-010-0202-6.

Abid, K., Zouari, K., Dulinski, M., Chkir, N., Abidi, B., 2011. Hydrologic and geologic factors controlling groundwater geochemistry in the Turonian aquifer (southern Tunisia). Hydrogeol. J. 19, 415–427. https://doi.org/10.1007/s10040-010-0668-z

Abouelmagd, A., Sultan, M., Milewski, A., Kehew, A.E., Sturchio, N.C., Soliman, F., Krishnamurthy, R. V, Cutrim, E., 2012. Toward a better understanding of palaeoclimatic regimes that recharged the fossil aquifers in North Africa: Inferences from stable isotope and remote sensing data. Palaeogeogr. Palaeoclimatol. Palaeoecol. 329, 137–149. https://doi.org/10.1016/j.palaeo.2012.02.024

Aissa, R.B., Boutoutaou, D., 2017. Characterization of groundwater in arid zones (Case of Ouargla basin). Energy Procedia 119, 556–564. https://doi.org/10.1016/j.egypro.2017.07.077

Alboghdady, M., El-Hendawy, S.E., 2016. Economic impacts of climate change and variability on agricultural production in the Middle East and North Africa region. Int. J. Clim. Chang. Strateg. Manag. https://doi.org/10.1108/IJCCSM-07-2015-0100

Alcalá, F.J., Custodio, E., 2008. Using the Cl/Br ratio as a tracer to identify the origin of salinity in aquifers in Spain and Portugal. J. Hydrol. 359, 189–207. https://doi.org/10.1016/j.jhydrol.2008.06.028

Aouad-Rizk, A., Job, J.L., Najem, W., Travi, Y., Blavoux, B., Gourcy, L., 2005. Oxygen-18 and deuterium contents over Mount Lebanon related to air mass trajectories and local parameters, in: Isotopic Composition of Precipitation in the Mediterranean Basin in Relation to Air Circulation Patterns and Climate. pp. 75–82. Climatic factors controlling chemical and isotopic characteristics of precipitation in Syria.

Aouidane, L., Belhamra, M., 2017. Hydrogeochemical processes in the Plio-Quaternary Remila aquifer (Khenchela, Algeria). J. African Earth Sci. 130, 38–47. http://dx.doi.org/10.1016/j.jafrearsci.2017.03.010

Appelo, C.A.J., Willemsen, A., 1987. Geochemical calculations and observations on salt water intrusions, I. A combined geochemical/minxing cell model. J. Hydrol. 94, 313–330. http://dx.doi.org/10.1016/0022-1694(87)90058-8

Beekman, H.E., 1991. Ion chromatography of fresh-and seawater intrusion: multicomponent dispersive and diffusive transport in groundwater. Febo. PhD Thesis, Free University of Amsterdam, The Netherlands, 198 pp.

Beguería, S., Vicente-Serrano, S.M., Reig, F., Latorre, B., 2014. Standardized precipitation evapotranspiration index (SPEI) revisited: parameter fitting, evapotranspiration models, tools, datasets and drought monitoring. Int. J. Climatol. 34, 3001–3023. https://doi.org/10.1002/joc.3887

Bekele, A., Schmerold, R., 2020. Characterization of brines and evaporite deposits for their lithium contents in the northern part of the Danakil Depression and in some selected areas of the Main Ethiopian Rift lakes. J. African Earth Sci. 170, 103904. https://doi.org/10.1016/j.jafrearsci.2020.103904.

Belkhiri, L., Mouni, L., Boudoukha, A., 2012. Geochemical evolution of groundwater in an alluvial aquifer: Case of El Eulma aquifer, East Algeria. J. African Earth Sci. 66–67, 46–55. https://doi.org/10.1016/j.jafrearsci.2012.03.001

Belkoum, N., Houha, B., 2017. Hydrochemistry and isotopic geochemistry contribution to the characterization of the aquifers of the upper Plains of Algeria, case of the basin of Chemora, oriental Algeria. J. Mater. Environ. Sci. 8, 3262–3268. http://www.jmaterenvironsci.com/Document/vol8/vol8_N9/346-JMES-3396-Belkoum.pdf

Belkoum, N., Houha, B., Rahal, O., 2020. Isotopic geochemistry utilization in the determination of the origin recharge rian upper plains lgeA of the water springs of the the algerian upper plains,. http://www.jmaterenvironsci.com/Journal/vol11-6.html

Benazzouz, M.T., 1986. Recherches géomorphologiques dans les hautes plaines de l'est algérien: la Sebkhet tarf (Algérie). PhD Thesis, Université Paris I, Sorbonne, 262 pg.

Bouchaou, L., Michelot, J.L., Vengosh, A., Hsissou, Y., Qurtobi, M., Gaye, C.B., Bullen, T.D., Zuppi, G.M., 2008. Application of multiple isotopic and geochemical tracers for investigation of recharge, salinization, and residence time of water in the Souss–Massa aquifer, southwest of Morocco. J. Hydrol. 352, 267–287. https://doi.org/10.1016/j.jhydrol.2008.01.022.

Bouchaou, L., Tagma, T., Boutaleb, S., Hssaisoune, M., El Morjani, Z.E.A., 2011. Climate change and its impacts on groundwater resources in Morocco: the case of the Souss-Massa basin. Climate Change Effects on Groundwater Resources - A Global Synthesis of Findings and Recommendations, Chapter 8, pp 129-143, CRC press, https://doi.org/10.1201/b11611

Bouragba, L., Mudry, J., Bouchaou, L., Hsissou, Y., Krimissa, M., Tagma, T., Michelot, J.L., 2011. Isotopes and groundwater management strategies under semi-arid area: case of the Souss upstream basin (Morocco). Appl. Radiat. Isot. 69, 1084–1093. https://doi.org/10.1016/j.apradiso.2011.01.041.

Bowen, G.J., Revenaugh, J., 2003. Interpolating the isotopic composition of modern meteoric precipitation. Water Resour. Res. 39. http://doi.org/10.129/2003WR002086.

Celle-Jeanton, H., Travi, Y., Blavoux, B., 2001. Isotopic typology of the precipitation in the Western Mediterranean region at three different time scales. Geophys. Res. Lett. 28, 1215–1218. https://doi.org/10.1029/2000GL012407

Christensen, J.H., Hewitson, B., Busuioc, A., Chen, A., Gao, X., Held, I., Jones, R., Kolli, R.K., Kwon, W.-T., Laprise, R., 2007. Regional climate projections. Chapter 11. The Physical Science Basis. Contribution of Working Group I to the Fourth Assessment Report of the Intergovernmental Panel on Climate Change [Solomon S., Qin D., Manning M., Chen Z., Marquis M., Averyt K.B., Tignor M., Miller H.L. (eds.)]. Cambridge University Press, Cambridge, United Kingdom and New York, NY, USA, pp 847–940, https://www.ipcc.ch/site/assets/uploads/2018/02/ar4-wg1-chapter11-1.pdf

Cook, B.I., Anchukaitis, K.J., Touchan, R., Meko, D.M., Cook, E.R., 2016. Spatiotemporal drought variability in the mediterranean over the last 900 years. J. Geophys. Res. 121, 2060–2074. https://doi.org/10.1002/2015JD023929https://doi.org/10.1002/2015JD023929

Craig, H., 1961. Isotopic variations in meteoric waters. Science 133, 1702–1703. https://doi.org/10.1126/science.133.3465.1702

Dansgaard, W., 1964. Stable isotopes in precipitation. Tellus 16, 436–468. https://doi.org/10.1111/j.2153-3490.1964.tb00181

Darling, W.G., Sorensen, J.P.R., Newell, A.J., Midgley, J., Benhamza, M., 2018. The age and origin of groundwater in the Great Western Erg sub-basin of the North-Western Sahara aquifer system: Insights from Krechba, central Algeria. Appl. Geochemistry 96, 277–286. https://doi.org/10.1016/j.apgeochem.2018.07.016

Demdoum, A., Hamed, Y., Feki, M., Hadji, R., Djebbar, M., 2015. Multi-tracer investigation of groundwater in El Eulma Basin (Northwestern Algeria), North Africa. Arab. J. Geosci. 8, 3321–3333. https://doi.org/10.1007/s12517-014-1377-z

Dib, D., Khiari, A., Kadi, K., Oualdjaoui, M., Gherraf, N., 2017. Identification of hydrogeochemical processes in a north eastern endoreic basin under semi-arid conditions (Algeria). http://dx.doi.org/10.4314/jfas.v9i3.28

Diffenbaugh, N.S., Giorgi, F., 2012. Climate change hotspots in the CMIP5 global climate model ensemble. Clim. Change 114, 813–822. https://doi.org/10.1007/s10584-012-0570-x

Durosoy G., 1956. Carte géologique de l'Algérie au 1/50.000éme, feuille N°206 Tébessa avec notice explicative détaillée, Pub. Serv. Carte Géol. Algérie.

Edmunds, W.M., Guendouz, A.H., Mamou, A., Moulla, A., Shand, P., Zouari, K., 2003. Groundwater evolution in the Continental Intercalaire aquifer of southern Algeria and Tunisia: trace element and isotopic indicators. Appl. geochemistry 18, 805–822. https://doi.org/10.1016/S0883-2927(02)00189-0.

Farid, I., Zouari, K., Rigane, A., Beji, R., 2015. Origin of the groundwater salinity and geochemical processes in detrital and carbonate aquifers: case of Chougafiya basin (Central Tunisia). J. Hydrol. 530, 508–532. https://doi.org/10.1016/j.jhydrol.2015.10.009

Gat, J.R., Dansgaard, W., 1972. Stable isotope survey of the fresh water occurrences in Israel and the northern Jordan Rift Valley. J. Hydrol. 16, 177–211. https://doi.org/10.1016/0022-1694(72)90052-2.

Gat, J.R., Gonfiantini, R., 1981. Stable isotope hydrology. Deuterium and oxygen-18 in the water cycle. Technical reports series 210, 339 p, IAEA, Vienna, ISBN 92-0-145281-0.

Ghodbane, M., Boudoukha, A., Benaabidate, L., 2015. Hydrochemical and statistical characterization of groundwater in the Chemora area, Northeastern Algeria. Desalin Water Treat 57: 14858–14868. https://doi.org/10.1080/19443994.2015.1067924

Gibson, J.J., Edwards, T.W.D., Bursey, G.G., Prowse, T.D., 1993. Estimating Evaporation Using Stable Isotopes: Quantitative Results and Sensitivity Analysis for Two Catchments in Northern Canada: Paper presented at the 9th Northern Res. Basin Symposium/Workshop (Whitehorse/Dawson/Inuvik, Canada-August 1992). Hydrol. Res. 24, 79–94. https://doi.org/10.2166/nh.1993.0015.

Giménez-Forcada, E., 2010. Dynamic of sea water interface using hydrochemical facies evolution diagram. Groundwater 48, 212–216. http://dx.doi.org/10.1111/j.1745-6584.2009.00649.x

Giménez-Forcada E., 2018. Utilización del diagrama de evolución de facies hidroquímica en los estudios sobre distribución de elementos traza en aguas subterráneas. In Navarro et al. (Eds), Proc. of "Agua subterránea, medio ambiente, salud y patrimonio", Congreso Ibérico. AIH-GE. Salamanca, November 2018, 597-602, ISBN: 978-84-938046-6-4

Giménez-Forcada E., Sánchez San Román F.J., 2015. An excel macro to plot the HFE-dia- gram to identify seawater intrusion phases. Groundwater 53:819–824. http://dx.doi.org/10.1111/gwat.12280.

Gonfiantini R., 1986. Isotopes in lake studies, in Handbook of Environmental Isotope Geochemistry (P. Fritz and J-Ch. Fontes, Eds.), Vol. 2, pp.113-168.

Guellal, S., Vila, J.M., 1973. Étude géologique du permis Aïn Beda. Rapp. Sonatrach, unpublished.

Guendouz, A., Moulla, A.S., 2010. The Shared Resources in the North-Western Sahara Aquifer System (Algeria-Tunisia-Libya): The use of Environmental Isotopes (Algeria part). Proceeding of the International Conference "Transboundary Aquifers: Challenges and New Directions" (ISARM2010), 1-4. Paris, 6-8 December 2010.

Guiraud R., 1977. Sur la néotectonique des régions Ouest-Constantinoises. Bull. Soc. Géol. France 7(3), 615-650.

Guttman, N.B., 1999. Accepting the stadardized precipitation index: a calculation algorithm. J. Am. Water Resour. Assoc. 35, 311–322. https://doi.org/10.1111/j.1752-1688.1999.tb03592.x

Haddadin M.J., 2001. Water scarcity impacts and potential conflicts in the MENA region. Water Int 26, 460–470. https://doi.org/10.1080/02508060108686947

Hadour, A., Mahé, G., Meddi, M., 2020. Watershed based hydrological evolution under climate change effect: An example from North Western Algeria. J. Hydrol. Reg. Stud. 28, 100671. https://doi.org/10.1016/j.ejrh.2020.100671

Harbi, A., Maouche, S., Ayadi, A., 1999. Neotectonics and associate seismicity in the Eastern Tellian Atlas of Algeria. J. Seismol. 3, 95–104. https://doi.org/10.1023/A:1009743404491

Helvacı, C., Palmer, M.R., 2017. Origin and distribution of evaporite borates: the primary economic sources of boron. Elem. An Int. Mag. Mineral. Geochemistry, Petrol. 13, 249–254. https://doi.org/10.2138/gselements.13.4.249

Hoerling, M., Eischeid, J., Perlwitz, J., Quan, X., Zhang, T., Pegion, P., 2012. On the increased frequency of Mediterranean drought. J. Clim. 25, 2146–2161. https://doi.org/10.1175/JCLI-D-11-00296.1.

IPCC, 2013. Climate Change 2013: The Physical Science Basis. Contribution of Working Group I to the Fifth Assessment Report of the Intergovernmental Panel on Climate Change [Stocker, T.F., D. Qin, G.-K. Plattner, M. Tignor, S.K. Allen, J. Boschung, A. Nauels, Y. Xia, V. Bex and P.M. Midgley (eds.)]. Cambridge University Press, Cambridge, United Kingdom and New York, NY, USA, 1535 pp.

Kahal, A., Saaidia, B., Chaab, S., Sayad, L., Chaffai, H., 2018. Hydrogeochemical characterization of a plain groundwater in a semi-arid area. Case of the F'Kirina aquifer (Northeastern Algeria). J. Bio. Env. Sci. 12(5), 432-440, ISSN: 2220-6663 (Print) 2222-3045 (Online), 12(5), 432-440. https://www.innspub.net/wp-content/uploads/2018/07/JBES-Vol-12-No-5-p-432-440.pdf

Kamel, S., 2013. Salinisation origin and hydrogeochemical behaviour of the Djerid oasis water table aquifer (southern Tunisia). Arab. J. Geosci. 6, 2103–2117. https://doi.org/10.1007/s12517-011-0502-5.

Laffitte, R., 1939. Etude géologique de l'Aurès. Service de la carte géologique de l'Algérie.

Lambrakis, N., Kallergis, G., 2001. Reaction of subsurface coastal aquifers to climate and land use changes in Greece: modelling of groundwater refreshening patterns under natural recharge conditions. J. Hydrol. 245, 19–31. https://doi.org/10.1016/S0022-1694(01)00334-1.

Leduc, C., Pulido-Bosch, A., Remini, B., 2017. Anthropization of groundwater resources in the Mediterranean region: processes and challenges. Hydrogeol. J. 25, 1529–1547. https://doi.org/10.1007/s10040-017-1572-6

Lelieveld, J., Proestos, Y., Hadjinicolaou, P., Tanarhte, M., Tyrlis, E., Zittis, G., 2016. Strongly increasing heat extremes in the Middle East and North Africa (MENA) in the 21st century. Clim. Change 137, 245–260. https://doi.org/10.1007/s10584-016-1665-6

Lionello, P., 2012. The climate of the Mediterranean region: From the past to the future. Elsevier. https://doi.org/10.1016/C2011-0-06210-5

Lloyd-Hughes, B., Saunders, M.A., 2002. A drought climatology for Europe. Int. J. Climatol. 22, 1571–1592. https://doi.org/https://doi.org/10.1002/joc.846https://doi.org/10.1002/joc.846

Marchina, C., Bianchini, G., Natali, C., Pennisi, M., Colombani, N., Tassinari, R., Knoeller, K., 2015. The Po river water from the Alps to the Adriatic Sea (Italy): new insights from geochemical and isotopic (δ 18 O-δD) data. Environ. Sci. Pollut. Res. 22, 5184–5203. http://doi.org/10.1007/s11356-014-3750-6.

Marchina, C., Zuecco, G., Chiogna, G., Bianchini, G., Carturan, L., Comiti, F., Engel, M., Natali, C., Borga, M., Penna, D., 2020. Alternative methods to determine the δ2H-δ18O relationship: An application to different water types. J. Hydrol. 587, 124951. https://doi.org/10.1016/j.jhydrol.2020.124951

Mariotti, A., Pan, Y., Zeng, N., Alessandri, A., 2015. Long-term climate change in the Mediterranean region in the midst of decadal variability. Clim. Dyn. 44, 1437–1456. https://doi.org/10.1007/s00382-015-2487-3

Marmi R., 1995. Les bassins continentaux de l'avant-pays de la chaîne alpine nord-orientale. Etude stratigraphique, sédimentaire, structurale et géochimique. Thèse de doctorat Université de Henri Poincaré, Nancy1, 283 pp.

McKee T.B., Doesken N.J., Kleist J., 1993, 1993. The relationship of drought frequency and duration to time scales, in: Proc. 8th Conf. on Applied Climatology, Anaheim, California, 179–184.

Mejri, S., Chekirbene, A., Tsujimura, M., Boughdiri, M., Mlayah, A., 2018. Tracing groundwater salinization processes in an inland aquifer: a hydrogeochemical and isotopic approach in Sminja aquifer (Zaghouan, northeast of Tunisia). J. African Earth Sci. 147, 511–522. https://doi.org/10.1016/j.jafrearsci.2018.07.009

Mertineit, M., Schramm, M., 2019. Lithium Occurrences in Brines from Two German Salt Deposits (Upper Permian) and First Results of Leaching Experiments. Minerals 9, 766. https://doi.org/10.3390/min9120766.

Merzouk Z., López Steinmetz R.L., Hacini M., Bing Fong S., M'nif A., Hamzaoui A.H., López Steinmetz L.C., 2020. Saharan lithium: Brine chemistry of chotts from eastern Algeria. App Geochem, 115, 104566. https://doi.org/10.1016/j.apgeochem.2020.104566.

Mokadem, N., Demdoum, A., Hamed, Y., Bouri, S., Hadji, R., Boyce, A., Laouar, R., Sâad, A., 2016. Hydrogeochemical and stable isotope data of groundwater of a multi-aquifer system: Northern Gafsa basin–Central Tunisia. J. African Earth Sci. 114, 174–191. https://doi.org/10.1016/j.jafrearsci.2015.11.010.

Natali, C., Bianchini, G., Marchina, C., Knöller, K., 2016. Geochemistry of the Adige River water from the Eastern Alps to the Adriatic Sea (Italy): evidences for distinct hydrological components and water-rock interactions. Environ. Sci. Pollut. Res. 23, 11677–11694. http://doi.org.10.1007/s11356-016-6356-3.

Potop, V., Boroneanţ, C., Možný, M., Štěpánek, P., Skalák, P., 2014. Observed spatiotemporal characteristics of drought on various time scales over the Czech Republic. Theor. Appl. Climatol. 115, 563–581. https://doi.org/10.1007/s00704-013-0908-y

Potop, V., Možný, M., Soukup, J., 2012. Drought evolution at various time scales in the lowland regions and their impact on vegetable crops in the Czech Republic. Agric. For. Meteorol. 156, 121–133. https://doi.org/10.1016/j.agrformet.2012.01.002

Re, V., Sacchi, E., Mas-Pla, J., Menció, A., El Amrani, N., 2014. Identifying the effects of human pressure on groundwater quality to support water management strategies in coastal regions: A multi-tracer and statistical approach (Bou-Areg region, Morocco). Sci. Total Environ. 500, 211–223. https://doi.org/10.1016/j.scitotenv.2014.08.115

Reiser, H., Kutiel, H., 2011. Rainfall uncertainty in the Mediterranean: time series, uncertainty, and extreme events. Theor. Appl. Climatol. 104, 357–375. https://doi.org/10.1007/s00704-010-0345-0

Robins, N.S., Calow, R.C., Macdonald, A.M., Macdonald, D.M.J., Gibbs, B.R., Orpen, W.R.G., Mtembezeka, P., Andrews, A.J., Appiah, S.O., Banda, K., 1997. Groundwater management in drought-prone areas of Africa. Final Rep., British Geological Survey Report WC/97/57.

Rozanski, K., Araguás-Araguás, L., Gonfiantini, R., 1993. Isotopic Patterns in Modern Global Precipitation. Geophysical Monograph Series 78, Climate Change in

Continental Isotopic Records (eds P.K. Swart, K.C. Lohmann, J. Mckenzie and S. Savin). https://doi.org/https://doi.org/10.1029/GM078p0001
Saighi O., 2005. Isotopic composition of precipitation from Algiers and Assekrem. In: Isotopic composition of precipitation in the Mediterranean Basin in relation to air circulation patterns and climate, Final report of a coordinated research project 2000–2004, IAEA-TECDOC-1453, IAEA, Vien, ISBN 92–0–105305–3, ISSN 1011–4289, 5-18, https://www-pub.iaea.org/MTCD/publications/PDF/te_1453_web.pdf
Saighi, O., Michelot, J.L., Filly, A., 2001. Isotopic characteristic of meteoric water and groundwater in Ahaggar massif (central Sahara). https://inis.iaea.org/collection/NCLCollectionStore/_Public/32/018/32018317.pdf?r=1
Salima, D., Belgacem, H., 2017. The hydrochemical characterization of the upper plains aquifers: case of the plain of F'kirina Ain-Beïda, Northeastern Algeria. Desalin. Water Treat. 92, 90–97. https://www.deswater.com/DWT_abstracts/vol_92/92_2017_90.pdf
Schilling, J., Freier, K.P., Hertig, E., Scheffran, J., 2012. Climate change, vulnerability and adaptation in North Africa with focus on Morocco. Agric. Ecosyst. Environ. 156, 12–26. https://doi.org/10.1016/j.agee.2012.04.021
Schulz, S., Horovitz, M., Rausch, R., Michelsen, N., Mallast, U., Köhne, M., Siebert, C., Schüth, C., Al-Saud, M., Merz, R., 2015. Groundwater evaporation from salt pans: examples from the eastern Arabian Peninsula. J. Hydrol. 531, 792–801. http://dx.doi.org/10.1016/j.jhydrol.2015.10.048
Souid, F., Telahigue, F., Agoubi, B., Kharroubi, A., 2020. Isotopic behavior and self-organizing maps for identifying groundwater salinization processes in Jerba Island, Tunisia. Environ. Earth Sci. 79, 1–10. https://doi.org/10.1007/s12665-020-8899-3
Sousa, P.M., Trigo, R.M., Aizpurua, P., Nieto, R., Gimeno, L., Garcia-Herrera, R., 2011. Trends and extremes of drought indices throughout the 20th century in the Mediterranean. Nat. Hazards Earth Syst. Sci. 11, 33–51. https://doi.org/10.5194/nhess-11-33-2011.
Tarki, M., Dassi, L., Jedoui, Y., 2012. Groundwater composition and recharge origin in the shallow aquifer of the Djerid oases, southern Tunisia: implications of return flow. Hydrol. Sci. J. 57, 790–804. https://doi.org/10.1080/02626667.2012.681783
UNESCO, UN-Water, 2020. United Nations World Water Development Report 2020: Water and Climate Change, Paris.
Vicente-Serrano, S.M., Beguería, S., López-Moreno, J.I., 2010. A multiscalar drought index sensitive to global warming: the standardized precipitation evapotranspiration index. J. Clim. 23, 1696–1718. https://doi.org/10.1175/2009JCLI2909.1.
Vila, J.M., 1977. Notice explicative de la carte géologique, au 1/50.000, Touffana (feuille n 202). Ed. par Sonatrach 6.
Vôute, C., 1967. Essai de synthèse de l'histoire géologique des environs d'Ain Fakroun, Ain Babouche et les régions limitrophes. Publication du service de cartes géologiques, NS. Bull 3.
Wilidi, W., 1983. La chaîne tello-rifaine (Algérie, Maroc, Tunisie): structure, stratigraphie et évolution du Trias au Miocène. Rev. géographie Phys. géologie Dyn. 24, 201–297.
Yang, W.H., Traut, B.H., Silver, W.L., 2015. Microbially mediated nitrogen retention and loss in a salt marsh soil. Ecosphere 6, 1–15. https://doi.org/10.1890/ES14-00179.1.
Younsi H. E., 2009. Epuisement de la nappe aquifère de la région de F'kirina (W. d'Oum El Bouaghi), et ces répercussions sur la gestion des ressources en eau). Memoire Dipl. Magister, Université Badji Mokhtar-Annaba, http://biblio.univ-annaba.dz/wp-content/uploads/2014/04/memoire-finale.pdf
Zatout, M., Steinmetz, R.L.L., Hacini, M., Fong, S.B., M'nif, A., Hamzaoui, A.H., Steinmetz, L.C.L., 2020. Saharan lithium: Brine chemistry of chotts from eastern Algeria. Appl. Geochemistry 115, 104566. https://doi.org/10.1016/j.apgeochem.2020.104566.

Zereg, S., Boudoukha, A., Benaabidate, L., 2018. Impacts of natural conditions and anthropogenic activities on groundwater quality in Tebessa plain, Algeria. Sustain. Environ. Res. 28, 340–349. https://doi.org/10.1016/j.serj.2018.05.003.

Zghibi, A., Tarhouni, J., Zouhri, L., 2013. Assessment of seawater intrusion and nitrate contamination on the groundwater quality in the Korba coastal plain of Cap-Bon (North-east of Tunisia). J. African Earth Sci. 87, 1–12. https://doi.org/10.1016/j.jafrearsci.2013.07.009